

UV REFLECTANCE OF FROSTS
COMPOSED OF WATER AND AMMONIA

By
John Gilbert Pipes

A DISSERTATION PRESENTED TO THE GRADUATE COUNCIL OF
THE UNIVERSITY OF FLORIDA IN PARTIAL
FULFILLMENT OF THE REQUIREMENTS FOR THE DEGREE OF
DOCTOR OF PHILOSOPHY

UNIVERSITY OF FLORIDA
1972

To my wife, Betty

ACKNOWLEDGMENTS

The author wishes to express his gratitude to Dr. R. C. Anderson, whose technical assistance, professional interest, and efforts put forth in obtaining the financial support for this study were far beyond the requirements of a committee chairman.

The author would like to thank Dr. A. E. S. Green, Dr. A. G. Smith, Dr. B. M. Leadon, Dr. M. H. Clarkson, and Dr. D. T. Williams for their efforts contributed as members of his supervisory committee.

Special acknowledgment is extended to Dr. T. G. McRae for his complete and accurate technical advice on vacuum system techniques.

The author would also like to acknowledge Mr. H. E. Stroud for his general assistance in procuring equipment and materials needed for the construction of the experimental apparatus.

This research was supported by the National Science Foundation, Grant GA28852.

TABLE OF CONTENTS

	Page
Acknowledgments	iii
List of Tables	v
List of Figures	vi
Abstract	viii
I. Introduction	1
A. Impetus	1
B. Design Considerations	3
C. Basic Results	5
II. Experimentation	7
A. Light Source	7
B. Monochromator	7
C. Frost Chamber	12
D. Photometry	13
E. Source Gases	21
III. H ₂ O and NH ₃ Frost UV Reflectivities	23
A. Frost Growth Procedures	23
B. NH ₃ Frost Results	25
C. H ₂ O Frost Results	29
IV. Conclusions	90
Appendices	94
Appendix Introduction	95
Appendix 1. Light Source	96
Appendix 2. Monochromator	100
Appendix 3. Frost Chamber	102
Appendix 4. Source Gases	104
Appendix 5. Calibration of PM Tubes	108
Bibliography	112
Biographical Sketch	115

LIST OF TABLES

Table	Page
1. Cross-Calibration Values	15
2. Gain-Volts Calibration Values	19
3. Reflectivity vs. Wavelength for NH_3 #9, 10, 11, and 12	38
4. Reflectivity vs. Wavelength for NH_3 #17a and b	41
5. Reflectivity vs. Wavelength for NH_3 #19a, b, and c	44
6. Reflectivity vs. Wavelength for H_2O #5a and b	60
7. Reflectivity vs. Wavelength for H_2O #7a and b	63
8. Reflectivity vs. Wavelength for H_2O #10a and b	66
9. Reflectivity vs. Wavelength for H_2O #12a and b	69
10. Reflectivity vs. Wavelength for H_2O #13a, b, c, and d	74
11. Reflectivity vs. Wavelength for H_2O #14a, b, c, and d	79

LIST OF FIGURES

Figure		Page
1.	The Schematic Diagram of the Experimental Arrangement	9
2.	The Photographs of the Experimental Arrangement and Light Source	11
3.	The Cross-Calibration Curve	14
4.	The Gain-Volt Calibration of PM 9553	18
5.	NH ₃ #9: Cubic Phase	31
6.	NH ₃ #10: Cubic Phase	33
7.	NH ₃ #11: Cubic Phase	35
8.	NH ₃ #12: Amorphous Phase	37
9.	NH ₃ #17a and b: Amorphous and Cubic Phases	40
10.	NH ₃ #19a, b, and c: Cubic Phase	43
11.	NH ₃ Gas Absorption Coefficients	45
12.	NH ₃ Solid Absorption Coefficients	46
13.	Photographs of Cubic and Amorphous NH ₃	48
14.	Photographs of NH ₃ Frosts Having Various Textures	50
15.	H ₂ O #5a and b: Cubic Phase	59
16.	H ₂ O #7a and b: Cubic Phase	62
17.	H ₂ O #10: (a), Amorphous Phase; (b), Cubic Phase	65
18.	H ₂ O #12: (a), Amorphous Phase; (b), Cubic Phase	68
19.	H ₂ O #13A: (a), Amorphous Phase	71

LIST OF FIGURES (continued)

Figure		Page
20.	H ₂ O #13: (b), (c), Cubic Phase; (d), NH ₃ Added Over H ₂ O Cubic	73
21.	H ₂ O #14: (a), Amorphous Phase	76
22.	H ₂ O #14: (b), (c), (d), Cubic Phase	78
23.	H ₂ O Vapor Absorption Coefficients	80
24.	H ₂ O Solid Hexagonal and Amorphous Absorption Coefficients	81
25.	BaSO ₄ and Stainless Steel Substrate Reflectivities	82
26.	Photographs of H ₂ O Cubic Frosts Grown with a Buffer Gas	84
27.	Photographs of H ₂ O Buffer-Gas-Frosts and H ₂ O Amorphous Frost	86
28.	H ₂ O "Ball" Frost Growth Sequence	88
29.	H ₂ O Phase Change Data	89
30.	Comparison of Jovian UV Albedo to NH ₃ Frost Reflectivity	93
31.	H ₂ Light Source Output as a Function of Wavelength	99
32.	Photomultiplier Photocathode Nonuniformities	110

Abstract of Dissertation Presented to the
Graduate Council of the University of Florida in Partial Fulfillment
of the Requirements for the Degree of Doctor of Philosophy

UV REFLECTANCE OF FROSTS
COMPOSED OF WATER AND AMMONIA

By

John Gilbert Pipes

June, 1972

Chairman: Dr. R. C. Anderson
Major Department: Aerospace Engineering

The reflectance spectra of ammonia and water frosts in the range 1400\AA to 3000\AA were measured near 77°K . For both gases the solid cubic and amorphous phases were examined. The cubic phase was established by slow warming of the amorphous frosts. For the ammonia frosts the cubic phase was also obtained by deposition of the gas at 180°K . The effects on frost reflectivity, of grain size and buffer gas during the growth period were studied. Both gases were deposited until the frosts were optically thick for 3000\AA radiation. The ammonia frosts have short wavelength cutoffs between 2100\AA and 2000\AA while the water frosts cut off at 1800\AA . Both the ammonia and water frosts exhibit increasing reflectivity toward shorter wavelengths. Water frosts have absorption minima centered at 2200\AA , 2075\AA , and 1925\AA while the ammonia frosts only show a continuum type absorption prior to the sharp cutoff. Reflectivities are less than 1 percent below 1900\AA in the case of ammonia and below 1700\AA in the case of water. Annealing of the cubic phase frosts resulted in a broadening and deepening of the absorption minima.

I. Introduction

A. Impetus

Middle ultraviolet spectra for most atoms and molecules in the gaseous phase, at least those relevant to the atmospheric sciences, have been recorded and in some instances data exist for the liquid and solid phase. The objective of the research report here was to determine the ultraviolet reflectivities of frosts composed of solid ammonia and water. The optical properties of atmospheric gases in the solid phase have been becoming increasingly important because of the renewed interest in the Jovian planets which has been prompted by the space program. Prime examples are the discussions by Pilcher et al. (1970), Kuiper et al. (1970a), and Kuiper et al. (1970b) of the Saturnian ring systems, believed to be covered by either an ammonia or water frost. These experimenters examined the near infrared and visible region while the OAO-2 (Wallace et al., 1972) recorded the Saturnian UV reflectivity down to 2250\AA . The temperature of the Saturnian rings is believed to be approximately 90°K (see Owen [1965], Harrison and Schoen [1967]).

In the case of Jupiter, Lewis (1969) has generated atmospheric models and concluded that ammonia ice clouds are present in the upper regions of the planet's atmosphere. In point of fact, it was this

very prediction of solid NH_3 clouds in conjunction with the UV rocket spectrum of Jupiter obtained by Anderson et al. (1969) that provided the impetus for this study.

Anderson et al. (1969) could not explain the sharp cutoff of the Jupiter albedo at 1800\AA using NH_3 gas and attributed it to an unknown absorber. Later, employing the absorption coefficient data of Dressler and Schnepf (1960) for solid cubic ammonia, Anderson and Pipes (1971) suggested the unknown Jovian constituent to be solid cubic ammonia. Since the data of Dressler and Schnepf (1960) for solid cubic ammonia consisted of only two data points in the wavelength region of interest, it was evident more experimental work on NH_3 solid was necessary.

It was thus proposed to grow NH_3 and H_2O frosts at LN_2 temperatures until they become optically thick for wavelengths near 3000\AA and to measure their reflectivities as far into the ultraviolet as experimentally possible. The apparatus design employed many of the experimental techniques used by the following investigators: Schnepf and Dressler (1960), studies of solid Xe, Kr, Ar; Kieffer (1968, 1969, 1970), spectral reflectance of $\text{CO}_2\text{-H}_2\text{O}$ frosts; and Wood et al. (1968, 1971), infrared reflectance of H_2O condensed on LN_2 -cooled surfaces. The work of Kieffer is by far most pertinent to the understanding of frosts, since the others were examining optical properties of micron thin clear ices or at best milky ices. Nevertheless, all these publications were extremely helpful in defining the experimental techniques employed in this study.

B. Design Considerations

A number of physical properties of NH_3 and H_2O had to be carefully considered during the experiment design. It is well established (Seiber et al., 1970; Dressler and Schnepf, 1960; Wood et al., 1971) that water has three distinct phases as a solid. The most common is the hexagonal structure which is obtained by freezing the liquid phase or by vapor deposition above 150°K . A cubic structure can be formed by vapor deposition at temperatures greater than 115°K and less than 150°K or by annealing the amorphous phase. Amorphous water is formed by vapor deposition at temperatures below 115°K .

In the case of ammonia, only the cubic and amorphous forms exist. Cubic ammonia is obtained from vapor deposition above approximately 140°K and below the melting point (195.3°K). Deposition at LN_2 temperatures results in amorphous ammonia. The amorphous phase seems to be the least understood configuration. Black et al. (1958) and Mauer et al. (1972) have conducted x-ray diffraction experiments on amorphous ammonia. Their results indicated that ammonia has two amorphous phases and that diffraction patterns indicative of cubic ammonia sometimes appear at 40°K for frosts grown at LHe temperature and subsequently allowed to slowly warm. Apparently, the deposition at LN_2 temperatures (77°K) does not assure a completely amorphous phase. This possibility was recognized and is discussed later after the phase change data are presented. Another very important conclusion by Mauer et al. (1971) is that once an amorphous phase is annealed into the cubic structure (warmed above 140°K) the amorphous phase

cannot be obtained again by cooling the cubic to temperatures as low as LHe.

An important aspect of frost spectroscopy is the characteristic equilibrium vapor pressure. Since the frosts are grown and examined in an evacuated chamber (typically 10^{-4} to 10^{-6} torr), it is essential that their vapor pressures at LN_2 temperatures is so low that absorption by vapor is insignificant. No experimental vapor pressure data exist for NH_3 and H_2O at 77°K ; however, calculated vapor pressures (see Appendix 4) are 10^{-25} torr for H_2O and 10^{-12} torr for NH_3 . Thus, the effect of gaseous absorption is unimportant.

Still another important consideration is the method of forming the frost. Vapor deposition on a cryogenic surface is classified as substrate cooling and is quite different from one of nature's prime cooling mechanisms, i.e., radiative cooling. In the laboratory the radiation is always a heat load on the frost instead of a heat loss; however, it is essentially impossible to cool every black or grey body surrounding the frost to temperatures lower than the frost. The conductive heat load must also be considered and is no doubt much larger than the radiative load even when the frost chamber is evacuated to 10^{-6} torr. This of course is assuming the walls of the chamber to be at room temperature. In short it would be difficult to simulate even approximately the frosts that exist in nature (e.g., Saturn's rings and the Martian polar cap); however, it is felt that valuable information can be extracted by growing frosts using substrate cooling.

C. Basic Results

The reflectivities of fourteen separate cubic and amorphous water frosts were recorded from 3000\AA to 1400\AA . All amorphous H_2O frosts were grown at LN_2 temperatures (77°K) while the growth rate, concentration of buffer gas, and substrate roughness were varied. The amorphous frosts appeared milky and very fine-grained. In almost every case the reflectivity was approximately 20 to 30 percent lower than the cubic structure frosts.

A cubic water frost was obtained by allowing an amorphous frost to warm gradually ($\frac{\Delta T}{\Delta t} \sim 4^\circ\text{deg/min}$) until the change of phase occurred at 150°K . The phase change was always accompanied by an exothermic reaction, a release of adsorbed noncondensable gases (the frost chamber pressure usually increased the order of $10\ \mu\text{Hg}$ over a background pressure of $5\ \mu\text{Hg}$), and an obvious increase in visible reflectivity.

The H_2O amorphous frost's reflectivity is relatively constant from 3000\AA to 2200\AA at which point the reflectivity decreases 20 percent in the region from 2200\AA to 1800\AA prior to the absorption cutoff at 1750\AA . Cubic water frosts exhibit an increasing reflectance from 3000\AA to 2300\AA and then three absorption features at 2200\AA , 2075\AA , and 1925\AA . The absorption cutoff is approximately the same for both water phases (1800\AA to 1700\AA) with the reflectivity dropping below 1 percent from 1700\AA to 1400\AA . No data were taken for the hexagonal structured solid water.

A total of nineteen ammonia frosts were grown; however, the results of the first four were inconclusive and only helped to establish experimental procedures. The same techniques for forming the H_2O

amorphous and cubic structures were employed for NH_3 , i.e., the amorphous frost was grown, reflectivities recorded, and then the frost was slowly warmed to the temperatures (150° to 180° K) required to obtain a transformation to the cubic structure. The exothermic reaction for the NH_3 amorphous to cubic phase change wasn't as abrupt as it was for H_2O so that only a small increase of the dewar warming rate was seen in the 130° K to 150° K range. Since the vapor pressure of NH_3 was increasing rapidly in this temperature range, no pressure fluctuation could be observed at the phase change. An exothermic process at the NH_3 phase change had also been observed by Black et al. (1958).

The NH_3 cubic and amorphous have similar reflectivities from 3000\AA to 2400\AA , i.e., an approximate increase of 30 percent toward shorter wavelengths. The reflectivity decreases rapidly below 2300\AA for the amorphous NH_3 and becomes less than 1 percent between 1950\AA and 1400\AA . For the NH_3 cubic the reflectance drops 30 percent from 2300\AA to 2275\AA , and then remains constant until the absorption cutoff at 2100\AA . This level region between 2275\AA and 2100\AA was not observed for NH_3 frosts when the deposition rates were sufficiently high so that latent heat loads cause the NH_3 cubic to be formed directly.

Unfortunately frosts composed of mixtures of NH_3 and H_2O could not be grown since NH_3 is extremely corrosive in the presence of H_2O .

In the following chapters a description of the experimental arrangement is given, and then the NH_3 and H_2O ultraviolet reflectivities are presented and discussed. A detailed description of the instrumentation is given in the appendices.

II. Experimentation

The experimental arrangement is shown schematically in Figure 1 and photographically in Figure 2. The experimentation is best described if subdivided into the following categories: A) the H_2 discharge light source, B) McPherson monochromator, C) frost chamber and cryosurface, D) Photometry, E) source gases.

A. Light Source

The light source was a flow-through electrodeless discharge type. Hydrogen was used as a discharge gas at pressures between 500 and 1000 μ Hg. Hydrogen exhibits a uniform continuum from 3000\AA to approximately 1650\AA so that little or no readjustment of the monochromator slits or photomultiplier tube gain was required. The source was placed sufficiently close to the entrance slit so that the optics of the monochromator were overfilled. The high temperature discharge gas was separated from the monochromator vacuum by a MgF_2 window. The source proved to be quite flexible, contamination free, and extremely stable for long periods of time. The spectral distribution of the light source is given in Appendix 1.

B. Monochromator

A 0.3m scanning McPherson monochromator was employed. The monochromatic energy requirements (never greater than 10^{-10} watts/cm²- \AA)

Figure 1. The Schematic Diagram of the Experimental Arrangement

- | | |
|--|---|
| A) Top Flange: Components: 1) high voltage and PM tube electrical feedthrough. 2) PM tube remote control. 3) thermocouple and ionization gauge. | J) Aluminum cold shield. |
| B) Front Flange: Components: 1) all gas inlet pipes. 2) holder for PM tube monitoring reflected radiation. 3) observation port. 4) outlet to MKS Baratron pressure transducer. | K) Monochromatic incident radiation. |
| C) Back Flange: Components: 1) LN ₂ inlet and outlet feedthroughs. 2) temperature thermocouple feedthrough. 3) roughing line vacuum valve. | L) Frost and reflected radiation |
| D) Six inch air operated gate valve. | M) LN ₂ reservoir. |
| E) Six inch chevron cryo-baffle. | N) LN ₂ inlet. |
| F) Six inch oil diffusion pump. | O) LN ₂ feedthroughs. |
| G) Cryo-surface | P) Connection flange containing pin hole and MgF ₂ window. |
| H) PM tube monitoring incident radiation. | Q) McPherson monochromator. |
| I) PM tube monitoring reflected radiation. | R) Two inch chevron cryo-baffle. |
| | S) Two inch oil diffusion pump. |
| | T) Outlet to mechanical vacuum pump |
| | U) One-half inch aluminum base plate. |

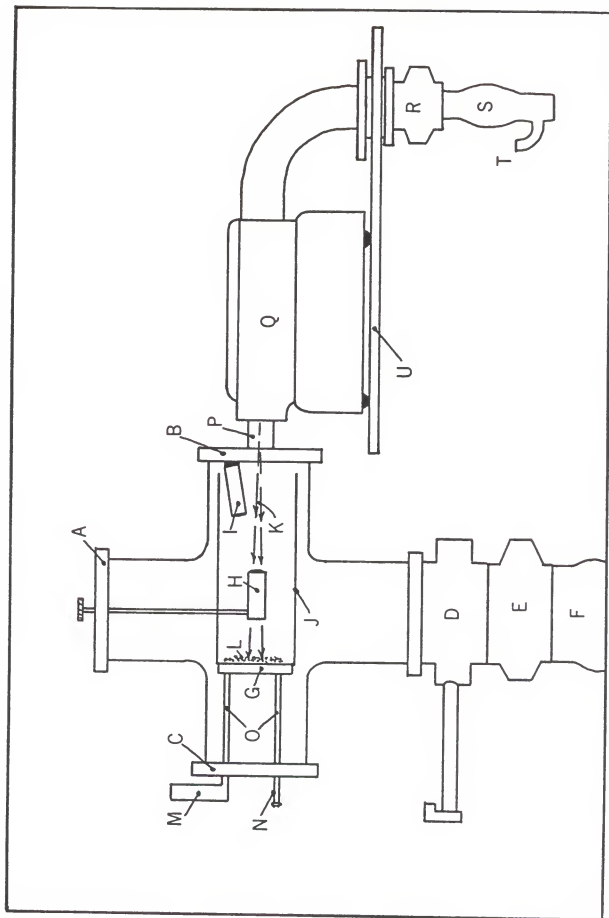


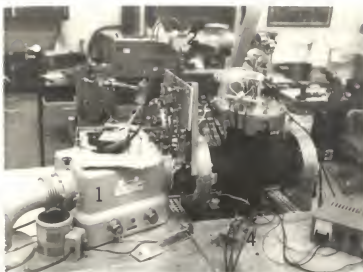
Figure 2. The Photographs of the Experimental
Arrangement and Light Source

A. Experimental Arrangement

Components labeled are: 1) McPherson monochromator. 2) MKS Baratron pressure transducer. 3) Frost chamber. 4) Preamplifier.

B. Light Source

Components labeled are: 1) H_2 discharge. 2) Microwave cavity. 3) Leak valve for inlet gas. 4) Outlet pipe to mechanical vacuum pump.



A



B

usually set the resolution at 26\AA° ; however, when the frost absorbed strongly the resolution was decreased to about 50\AA° . The scattered light from the monochromator was measured with a solar-blind photomultiplier tube and found to be negligible. To prevent the emergent beam from overfilling the photomultiplier tube used to measure the incident radiation (I_0), the f/5.3 beam of the McPherson was stopped down by a pin hole located between the monochromator and the frost chamber. The resulting beam formed a $1/2$ " diameter spot on the I_0 photomultiplier tube and a 1" diameter spot on the frost.

C. Frost Chamber

A six-inch Pyrex cross formed the vacuum chamber for frost growth and photometry. The four flanged ports were used to allow monochromatic light in, to control the position of the incident light photomultiplier tube, to connect to the vacuum diffusion pump, and to support the cryosurface. The flange arrangements are shown in Figure 1. The outside of the Pyrex cross was painted black and was also covered with a doublewalled black cloth which enabled the experiments to be conducted in room lighting. Chamber pressure was monitored by a thermocouple gauge, an ionization gauge, and a MKS Baratron 3mmHg transducer unit. After the frosts were grown, the chamber pressure was held at 10^{-6} torr while photometric data were taken.

Different cryosurfaces were used during the experimentation period. Primarily, rough and polished stainless steel frost dewars were used but for some experiments a copper dewar was substituted.

The frost dewar was connected to LN_2 vacuum feedthroughs to prevent O-ring freeze out and was fed from a 25 liter LN_2 supply dewar. The temperature of the frost dewar was monitored by an iron-constantan thermocouple silver soldered to its front surface.

D. Photometry

Two EMR 541F-05M-18 solar-blind photomultiplier tubes (hereafter denoted PM tubes) were positioned within the frost chamber to record the incident and reflected UV radiation. These PM tubes are sensitive to radiation with wavelengths between 3400\AA and 1400\AA . Each PM tube output was connected to a Fairchild solid-state preamplifier with a $\times 1$ gain and a low pass filter. After amplification and filtering, the PM tube output was displayed on a chart recorder and a digital volt meter. High voltage was provided by a Fluke 0-6000 volt power supply.

One of the PM tubes could be moved remotely into the beam to record the total incoming flux while the second PM tube was mounted to collect the reflected light at approximately 10° from normal incidence (see Figure 1). The monochromator was dialed to the desired wavelength and the total incident flux was measured. The PM tube used to record this signal was then moved out of the beam and the reflected light measured. This basic procedure was continued until all wavelengths were covered. Wavelength steps of 100\AA were used if the frost reflectivities were a continuum ($\lambda > 2400\text{\AA}$) and steps of 25\AA were used if reflectivities exhibited features and absorption cutoffs.

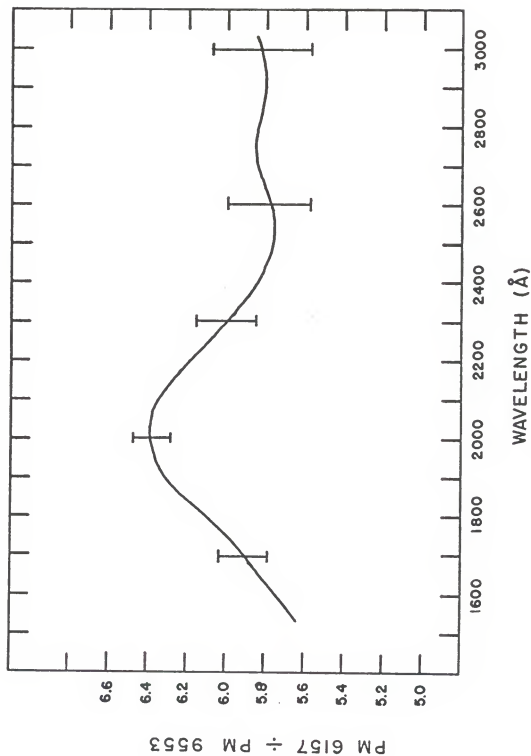


Figure 3. The Cross-Calibration Curve. PM 6157 is the reflected light detector and PM 9553 is the incident light detector.

Table 1
Cross-Calibration Values

Wavelength	PM 6157 ÷ PM 9553
3000	5.83
2900	5.81
2800	5.84
2700	5.85
2600	5.78
2500	5.78
2475	5.79
2450	5.80
2425	5.81
2400	5.84
2375	5.87
2350	5.91
2325	5.96
2300	6.00
2275	6.05
2250	6.09
2225	6.14
2200	6.19
2175	6.23
2150	6.27
2125	6.31
2100	6.35
2075	6.37
2050	6.38
2025	6.39
2000	6.38
1975	6.37
1950	6.36
1925	6.34
1900	6.31
1875	6.27
1850	6.21
1825	6.16
1800	6.10
1775	6.06
1750	6.00
1725	5.96
1700	5.91

Since the spectral sensitivity of the two PM tubes are different they had to be cross calibrated. This calibration is needed in order to calculate what the incident light would have registered on the PM tube used to measure the reflected light. The cross-calibration was determined by placing the PM tubes side by side facing the UV beam. For some constant monochromatic incident flux the tubes were moved in and out of the beam and the resulting outputs were divided. The cross-calibration curve is shown in Figure 3 with the appropriate error bars and the values are listed in Table 1. The cross-calibration errors are essentially the total errors of the experiment and are a result of nonuniformities in the UV beam and the PM photocathodes. These nonuniformity problems were of great concern and are discussed in Appendix 5.

Calculation of the expected signal levels showed that the PM tube used to measure the incident radiation could be saturated while the PM measuring the reflected radiation would have a low signal-to-noise ratio. This problem is a direct result of the reflectance characteristics of the frost. It is assumed that the frost is a Lambert reflector and thus distributes the incident flux according to the cosine law. The angular distribution of reflected radiation from CO₂ cryodeposits has been measured by Smith et al. (1969) and was found to be essentially Lambertian. As positioned in the chamber, the reflected light PM tube had a collecting solid angle approximately 10^{-3} times that of a hemisphere and thus the intensity of radiation on the reflected light PM tube was $\sim 10^{-3}$ that of the incident light PM tube. This difficulty was overcome by operating the incident light

PM tube at a reduced gain compared to the reflected light PM tube. The PM tube gain was controlled by varying the applied high voltage. The reflected light PM tube was always kept at 2950 volts while the incident light PM tube high voltage ranged from 1600 to 2800 volts.

Following this procedure of reducing the gain of one PM tube meant that a gain-volt calibration for this particular tube had to be established so that measurements taken at a reduced gain could be accurately extrapolated to the gain at 2950 volts. This was easily accomplished by parking the PM tube in the light beam and changing the applied high voltage over a broad range (1600-2950 volts). Next, all PM tube outputs at reduced voltages were divided into the output at 2950 volts. This function is plotted in Figure 4 and tabulated in Table 2. It was found that signals at 2950 volts could be readily predicted within an accuracy of ± 1 percent by recording the signals at reduced voltages. In most instances the voltage of the incident light PM tube ranged between 2400 and 2800 volts, and only in cases where large incident light levels were required to obtain a respectable reflected light signal (i.e., in wavelength regions of strong frost absorption) did the high voltage have to be reduced to 1600 to 1800 volts. For this case the error is somewhat worse (± 3 percent). The ± 1 percent accuracy in the 2400 to 2800 volt range is attributed to the highly commendable performance of the EMR solar-blind PM tube. This gain-volt calibration was checked from time to time during the experimental period and was always found to display this remarkable accuracy.

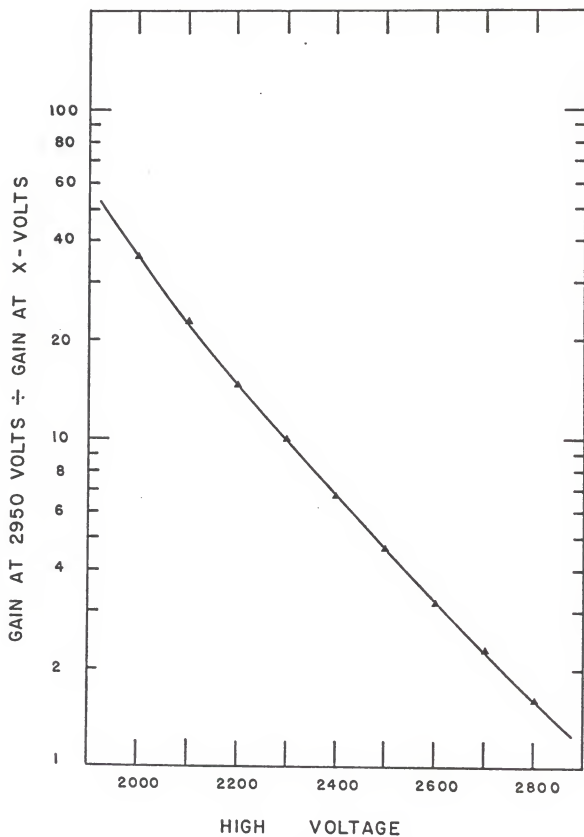


Figure 4. The Gain-Volt Calibration of PM 9553.

Table 2
Gain-Volts Calibration Values

X-High Voltage	Ratio $\frac{\text{Gain @ 2950 volts}}{\text{Gain @ x-volts}}$
1700	144.44
1800	92.86
1900	57.52
2000	35.14
2100	22.81
2200	14.77
2300	10.00
2400	6.67
2500	4.64
2600	3.17
2700	2.28
2800	1.60
2900	1.16
2950	1.00

Since the reflected light PM tube was stationary at 10° from normal incidence, the total hemispherical reflectance could only be measured by replacing the unknown reflector (NH_3 and H_2O frosts) by a diffusely reflecting standard. This was only done for 3000\AA radiation to establish a hemispherical reflectance and then all the remaining wavelengths were adjusted from a relative to an absolute reflectivity.

Initially magnesium oxide was chosen as a standard. Magnesium ribbon was burned and the oxide smoke collected on aluminum or stainless steel plates. However, after some laboratory use and a review of the literature, it was clear that magnesium oxide has a number of undesirable characteristics such as rapid aging, large thicknesses are required for opacity, the powder is quite fragile, and an uncertainty in the value of total reflectivity at 3000\AA (see Benford et al., 1948a and 1948b). It was thus decided to replace the magnesium oxide with a barium sulfate standard. In contrast to magnesium oxide, barium sulfate has the desirable properties of small changes in reflectance with age, it can be purchased commercially as a powder or as a paint from Eastman Kodak, and the paint is fairly durable. The reflectivities of aged BaSO_4 paint, fresh BaSO_4 paint, and BaSO_4 powder that was measured in this study are shown in Figure 25. The photometry of BaSO_4 from 2000\AA to 8000\AA is discussed in detail by Billmeyer (1969), Grum and Luckey (1968), and in Kodak publications No. JJ-31 and No. JJ-32.

A summary of the photometric procedure is as follows (the incident and reflected light PM tubes are denoted by their respective serial numbers, 9553 and 6157):

- 1) Measure $I_0 (\lambda)$ with PM 9553 at reduced gain (x-volts).
- 2) Calculate the $I_0 (\lambda)$ which PM 9553 would register at 2950 highvolts using the volts-gain calibration curve.
- 3) Employ the cross calibration curve to determine $I_0 (\lambda)$ which PM 6157 would have registered.
- 4) Measure $I_r (\lambda)$, the reflected light signal, with PM 6157, and divided it by $I_0 (\lambda)$ of step 3.
- 5) Adjust the relative reflectivity ($I_r [\lambda]/I_0 [\lambda]$), to a hemispherical reflectivity by comparison to $BaSO_4$ at 3000Å.

E. Source Gases

Ultrahigh pure ammonia (99.999 percent pure) was purchased commercially from Air Products and Chemicals Inc. and proved to be sufficiently pure. The primary foreign gas in the UHP ammonia is nitrogen which is noncondensable at 77° K and was thus pumped out by the diffusion pump during the frost growth. The NH_3 source bottle was connected to a ballast chamber and subsequently bled into the frost chamber through a needle valve.

Obtaining pure water vapor was somewhat more difficult than NH_3 . A commercial still was used to produce "conductivity water" which was collected in a glass vacuum trap. This trap was cleaned with chromic acid and leached with water from the still (approximately 200° F). After sufficient leaching, the water was collected in the trap and tested with a conductivity meter. A conductivity of 0.5×10^{-6} ohm⁻¹ cm⁻¹ was set as an acceptable purity.

The most difficult impurity to remove from water is ammonia absorbed in the form of NH_4OH . If the concentration of NH_4OH is very small it is totally dissociated into NH_4^+ and OH^- ions which are the ions measured with the conductivity meter. From order-of-magnitude calculations it can be shown (see Appendix 4) that for a conductivity of $0.5 \times 10^{-6} \text{ ohm}^{-1} \text{ cm}^{-1}$ the NH_4^+ ion concentration is approximately 0.2 ppm. This level of ammonia contamination in the water is much too small to be seen in the H_2O frost spectrum. It is possible that a greater amount of NH_3 was introduced into the H_2O frost by out-gassing of previously adsorbed NH_3 (from the chamber walls). This NH_3 out-gassing could only have been the order of 10 ppm which would still be undetectable in H_2O frost reflectivities.

Once the conductivity water was collected, the trap was immediately connected to the frost chamber inlet line and also to a mechanical vacuum pump line. This vacuum pump was activated so that the hot water boiled under vacuum. This process removed most of the nitrogen from the water and once the trap was valved off it contained pure water and a small amount of N_2 . During the H_2O frost growth the trap became cold due to the latent heat of evaporation and had to be warmed slightly in order to maintain the room temperature H_2O vapor pressure of 20 mmHg, thus insuring a uniform flow rate of H_2O vapor into the frost chamber.

III. H₂O and NH₃ Frost UV Reflectivities

A. Frost Growth Procedures

The techniques of controlling the growth environment for both NH₃ and H₂O were strictly a result of trial and error. The understanding of how to control effectively the closely coupled parameters of latent heat, heat transfer characteristics of the frosts, vapor pressure-temperature relationships, and phases of the solids was soon found to be more difficult than the recording of photometric data. It became increasingly obvious that the initial growing conditions (flow rate, chamber pressure, substrate roughness) dictated to a large extent the growth patterns for the remaining growth period. It was also recognized that it would be difficult to define these initial conditions. Particularly for NH₃, the establishment of whether the frost was in an amorphous or a cubic phase, or a combination of these two, was a major experimental problem.

From the works of Dressler and Schnepf (1960), Mauer et al. (1972), and Black et al. (1958), the techniques for obtaining an essentially complete amorphous phase are well established. The data of Dressler and Schnepf show that the solid cubic ammonia begins to absorb about 200Å deeper into the UV than the amorphous solid (see Figure 12). Early data taken herein always showed that both the amorphous and cubic frosts absorb strongly between 2200Å and 2000Å.

The early procedure for obtaining the NH_3 cubic structure was to keep the substrate temperature between 150°K and 190°K and to have a large growth rate. The reflectivities of these cubic NH_3 frosts always agreed with the amorphous frost reflectivity and thus some question of the phase was evident. This problem is discussed later after the NH_3 data are presented.

Once the H_2O frosts were grown, it was clear that the most convincing technique of assuring a particular phase was to grow the amorphous form first at a very slow rate and, after taking reflectance measurements, to anneal the amorphous form to a cubic form. The H_2O phase change was visually obvious but temperature and pressure data were recorded to substantiate the change (see Figure 29).

Another frost growing technique established through experimentation was whether the chamber should be closed off or whether it should be pumped on with the six-inch diffusion pump during the growth period. For the NH_3 and H_2O sources, foreign gases were of sufficient quantity that after a three-hour growth period a sealed frost chamber would have a buffer gas present which would considerably alter the growth conditions. The basic effect of a buffer (or noncondensable) gas during frost growth is to favor the growth of any frost particles protruding from the surface since these particles see a larger concentration to the condensable gas. The obvious decision was to leave the vacuum pump open to the chamber if the effects of a buffer gas were not desired.

For most of the latest NH_3 and H_2O frosts, the following growth procedure was followed:

- 1) Frost chamber pumped to 10^{-6} torr (on occasion the flanges were baked out at $T \sim 100^{\circ} \text{F}$).
- 2) Frost dewar cooled down to LN_2 temperature.
- 3) Flow started with vacuum pump on chamber. The chamber pressure was never above 10^{-3} torr during the growth period.
- 4) Stop flow and measure reflectance at 3000\AA . If it was comparable to the BaSO_4 reference, the frost was assumed to be optically thick; if not, the flow was turned back on.

The mass flow rate through the needle valve was never measured since it was impossible to determine what percentage of NH_3 or H_2O was being frozen on the cryosurface or pumped out by the diffusion pump. Also, the area of the cryosurface was poorly defined so that even if the mass flow rate was known a thickness or density measurement would have large errors. The chamber pressure was used as an indicator of the flow rate.

B. NH_3 Frost Results

The UV reflectivity measurements of NH_3 cubic and amorphous frosts are presented in Figures 5 through 10. Each figure caption gives pertinent information about the growth conditions. In addition, reflectivity data for each frost are shown in tabular form in Tables 3-5. Smooth curves were drawn through the data points listed in each table. Where zeros appear in the tables no data were taken. For comparison the gaseous NH_3 data of Watanabe et al. (1953) and the solid NH_3 data of Dressler and Schnepf have been reproduced in Figures 11 and 12.

The most striking result was the reflectivity exceeding 100 percent for frosts optically thick at 3000\AA . There are two possible causes for this result; one is a consistent error in photometry due to PM calibration errors and the second is that the frosts were not Lambert reflectors for radiation in the middle ultraviolet. It must also be mentioned that the different frost thicknesses for each experiment can introduce a maximum uncertainty of 5 percent for all wavelengths. For the thicker frosts the PM tube monitoring the reflected light was closer to the frosts and thus had a larger collecting solid angle while the PM tube measuring the incident flux always collected the total light on the frost. This effect can be seen at 3000\AA where the reflectivity differs from frost to frost.

As for the spectral variations in reflectivity the uncertainty lies in the Lambert assumption or calibration errors. On review of the cross-calibration curve it is clear that at best the spectral variance of reflectivity could be flat or increasing toward shorter wavelengths, corresponding to negative or positive calibration errors, respectively. As discussed in Appendix 5, the errors in cross-calibration were found to stem from nonuniformities of the PM tube photocathodes and little could be done to correct this problem; however, it seems safe to conclude that the reflectivities of both NH_3 and H_2O cubic frosts increased toward shorter wavelengths. Supporting evidence for this conclusion is the fact that some of the amorphous frosts were indeed found to be constant in spectral reflectivity in the wavelength region of no absorption.

It is just as possible that the frosts do not diffusely reflect as a Lambert surface for UV wavelengths and have a scattering phase function somewhat characteristic of a Rayleigh scattering media. This would result in a higher reflectivity near normal incidence than that of a Lambert reflector (e.g., the BaSO_4 reference). Unfortunately this possibility of an unknown scattering phase function could not be examined in this experiment since it would require recording the reflectivity at all reflecting angles, a task beyond the capabilities of the system.

For the wavelength region below 2400\AA the ammonia frosts were easily divisible into three groups: Group 1: NH_3 #9, 10, and 19 are cubic frosts that were grown directly into the cubic phase, Group 2: NH_3 #11 and 17b are cubic frosts formed by warming the amorphous deposits until they were within the phase change temperature range (when data were taken the frosts were recooled to 77°K), and Group 3: NH_3 #12 and 17a are amorphous frosts.

Group 3 shows no structure other than a continuum type cutoff from 2400\AA to 1950\AA and then was black out to 1400\AA (at 1600\AA the light source had sufficient output so that some return light could be measured and the result was a reflectivity less than 1 percent which was termed "black").

The Groups 1 and 2 were both cubic NH_3 frosts but Group 2 showed a reduction of 20 percent in reflectivity between 2400\AA and 2200\AA and then a decrease of only 10 percent in reflectivity for the next 100\AA prior to the sharp cutoff between 2100\AA and 2000\AA . Why this

sharp drop in reflectivity between 2300\AA and 2200\AA and a lesser decrease between 2200\AA and 2100\AA occurred in NH_3 cubic frosts formed by annealing from the amorphous phase could not be explained but is thought to be related to the percentage of cubic structure obtained by annealing as opposed to growing the cubic structure directly. The physics of these phase changes clearly warrants further attention and could be best studied by x-ray diffraction techniques.

For NH_3 #19, a cubic frost formed directly as a result of a large latent heat of formation load, the reflectivity has been plotted to exemplify the repeatability of the photometric data (see Figure 10). Three complete wavelength scans of the frost were made at one-hour intervals. The vacuum pump was open to the frost chamber for the entire three-hour period and the frost was kept at 77°K . The uncertainty in reflectivity is approximately ± 1.5 percent for $\lambda > 2400\text{\AA}$ and approximately ± 3 percent for $\lambda < 2400\text{\AA}$.

If the solid NH_3 absorption data of Dressler and Schnepf (Figure 12) are examined it is immediately obvious that one would anticipate a cubic frost to start absorption about 200\AA deeper in the UV than an amorphous frost. On the contrary the cubic NH_3 is observed to reflect only 80\AA farther into UV than the amorphous NH_3 (see Figure 9) and in some cases the cutoffs are essentially identical (see Figures 6, 7, and 8).

It was because of the cubic NH_3 absorption cutoff that in the early NH_3 experiments the question of what phase was being examined arose. Since the results of Dressler and Schnepf give cubic NH_3 absorption data only at 1875\AA , 1775\AA , and 1500\AA , the absorption

coefficients longward of 1875\AA obtained by an extrapolation are uncertain. The cubic NH_3 frosts grown by annealing the amorphous frosts show higher reflectivities at shorter wavelengths than those formed directly into the cubic phase. However, the cubic NH_3 of Dressler and Schnepf was formed at a high temperature, not by annealing of the amorphous NH_3 , and once again there appears to be conflict.

This discrepancy is difficult to analyze since amorphous NH_3 obtained by deposition at 77°K could quite possibly have contained an unknown amount of cubic NH_3 and vice versa. This reasoning follows from the x-ray work of Mauer et al. (1972). At best it can only be concluded that a large percentage of what was assumed to be amorphous phase was indeed amorphous. The technique followed in this study for preparing the separate phases is given by Mauer. The only absolute assurance of phase is to examine the solid NH_3 with x-ray patterns prior to measuring the UV reflectivities. Unfortunately this is beyond the scope of this research. All of these arguments are likewise applicable to the H_2O frosts.

Photographs taken during the growth of the NH_3 frosts and after annealing are shown in Figures 13 and 14. In all photographs the enlargement is a factor of two. Explanations of each are given in the figure captions.

C. H_2O Frost Results

The UV reflectivity measurements of H_2O cubic and amorphous frosts are presented in Figures 15 through 22. The H_2O amorphous and cubic results are presented separately in cases where the cubic frosts were

Figure 5. NH_3 #9: Cubic Phase

NOTES

- a) This frost was grown directly as solid cubic by deposition at 180°K .
- b) Buffer gas was He at $1000 \mu \text{Hg}$.
- c) Chamber was closed during recoiling to 77°K .
- d) Photometric data were taken at 77°K frost temperature.
- e) Photograph of this frost shown in Figures 13c and d.
- f) Resolution is given at top of the figure.
- g) Growth period 67 minutes.

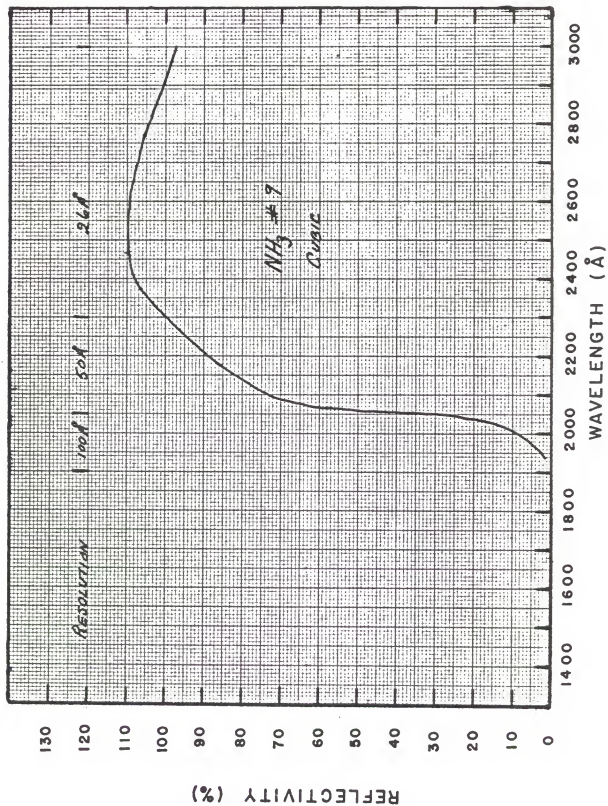


Figure 6. NH_3 #10: Cubic Phase

NOTES

- a) Frost was formed by very rapid deposition at 77°K . Result was cubic NH_3 .
- b) No buffer gas present.
- c) Chamber closed.
- d) Growth period 43 minutes.
- e) Visual inspection showed NH_3 crystals and extreme uniformity across frost dewar.

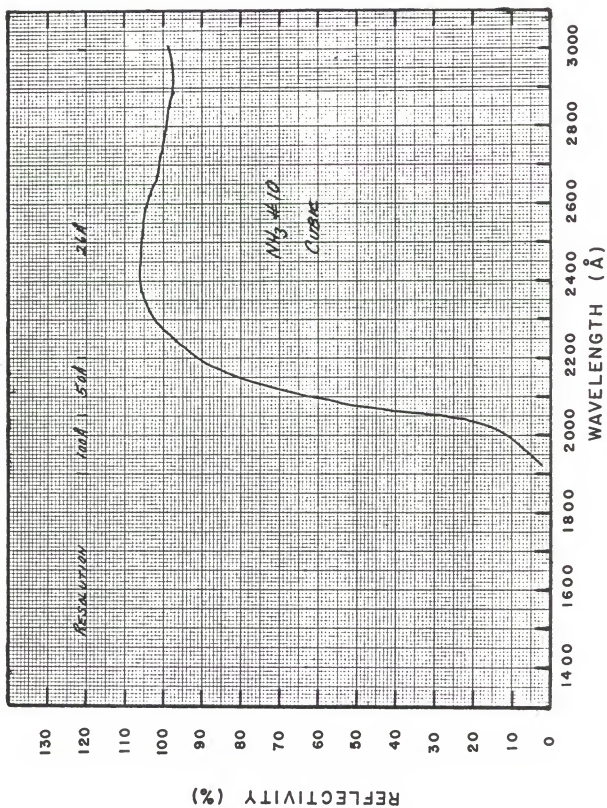


Figure 7. NH_3 #11: Cubic Phase

NOTES

- a) The phase was established by annealing the amorphous phase at $\sim 190^\circ\text{K}$.
- b) Frost recooled with chamber closed to 77°K .
- c) No buffer gas.
- d) Amorphous was formed by very slow deposition at 77°K .
- e) Growth period 3 hours 26 minutes.
- f) Chamber pressure $\sim 10^{-6}$ torr when photometric data were recorded.
- g) Note shoulder in reflectivity at 2200\AA .

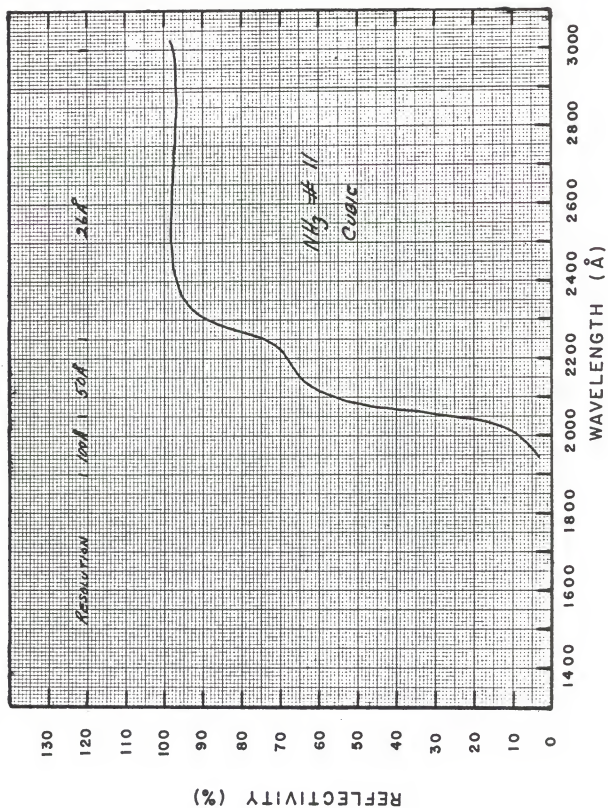


Figure 8. NH_3 #12: Amorphous Phase

NOTES

- a) Amorphous phase formed by very slow deposition at 77°K .
- b) Growth period 4 hours
- c) No buffer gas.
- d) Chamber open to vacuum pump.
- e) Visual inspection showed very fine-grained texture.
- f) Photograph of this frost shown in Figures 13a and b.

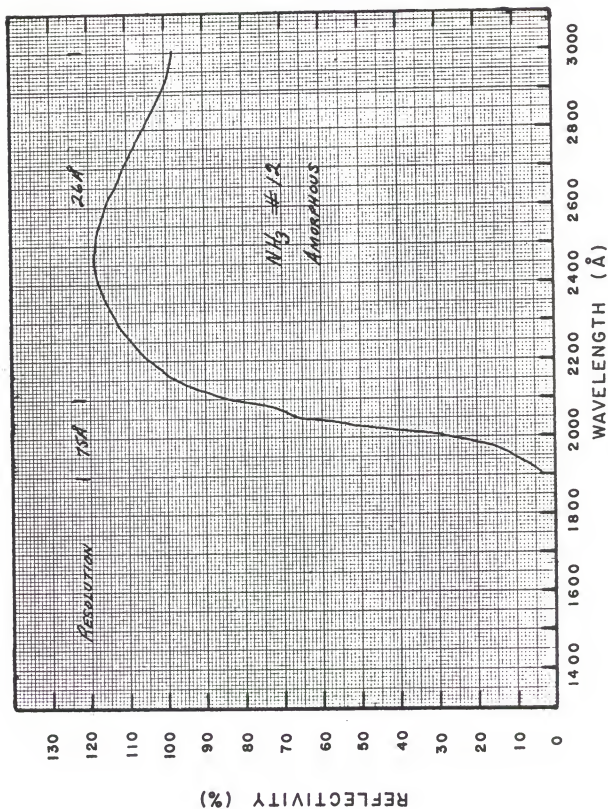


Table 3

-38-

Reflectivity vs. Wavelength
for NH₃ #9, 10, 11, and 12

1

WAVELENGTH	NH3 9	NH3 10	NH3 11	NH3 12
3000.	98.59	98.53	100.14	98.26
2900.	101.14	97.15	96.28	100.57
2800.	104.27	98.99	98.37	107.33
2700.	110.94	100.83	97.89	107.33
2600.	109.17	104.35	98.21	117.30
2500.	112.50	105.26	95.31	75.29
2475.	0.0	0.0	0.0	0.0
2450.	0.0	0.0	0.0	0.0
2425.	0.0	0.0	0.0	0.0
2400.	111.52	106.18	100.79	80.28
2375.	107.41	0.0	0.0	0.0
2350.	0.0	0.0	94.99	0.0
2325.	0.0	0.0	0.0	0.0
2300.	0.0	102.66	90.96	113.21
2275.	97.22	0.0	81.30	0.0
2250.	94.86	98.23	76.64	0.0
2225.	81.93	95.01	69.23	0.0
2200.	88.98	95.01	69.55	105.73
2175.	85.65	87.97	66.98	0.0
2150.	83.50	84.91	66.33	97.54
2125.	79.58	73.90	60.21	94.52
2100.	75.66	65.94	57.48	85.44
2075.	64.68	53.09	47.17	72.98
2050.	40.38	35.95	30.27	66.75
2025.	15.29	17.75	12.07	47.53
2000.	9.02	11.47	8.05	27.95
1975.	5.88	8.72	6.76	16.20
1950.	0.0	8.11	0.0	10.68

Figure 9. NH_3 #17a and b: Amorphous and Cubic Phases

NOTES

- a) NH_3 #17a is amorphous phase. #17b is cubic phase obtained by annealing amorphous frost at 190° K.
- b) No buffer gas. Chamber open to vacuum pump during amorphous growth.
- c) Chamber pressure 2×10^{-4} torr during deposition and 10^{-6} torr when photometric data were taken.
- d) Note shoulder in cubic frost reflectivity at 2200\AA and difference in reflectivity short of 2200\AA between amorphous and cubic.
- e) The reflectivity of the copper substrate used in some of the NH_3 frosts is also shown.

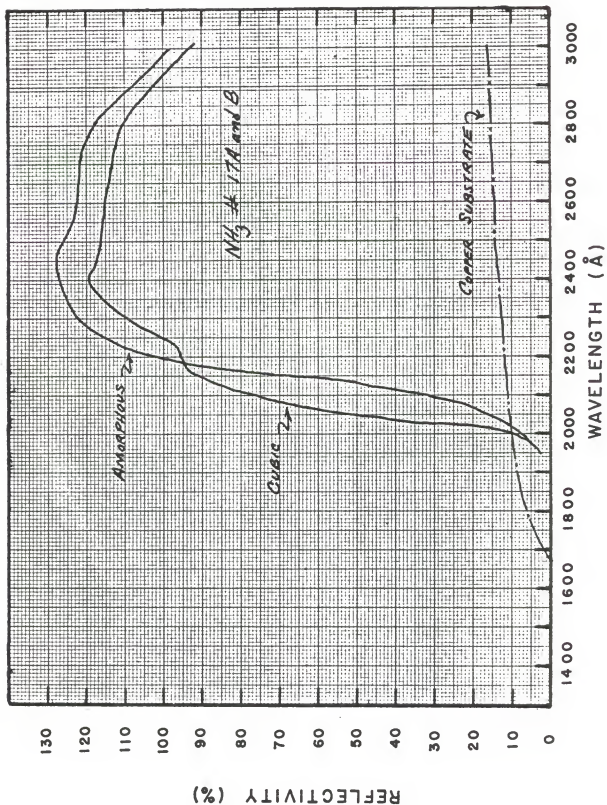


Table 4

-41-

Reflectivity vs. Wavelength for
 NH_3 #17a and b.

WAVELENGTH	NH3 17A	NH3 17B
3000.	98.60	92.96
2900.	108.07	103.58
2800.	119.52	112.88
2700.	122.51	113.21
2600.	122.18	116.03
2500.	125.66	116.37
2475.	127.82	117.36
2450.	128.32	117.69
2425.	129.31	118.86
2400.	126.33	120.68
2375.	126.49	119.35
2350.	125.33	118.86
2325.	125.83	114.87
2300.	122.67	112.38
2275.	120.85	107.57
2250.	115.70	102.42
2225.	112.55	97.94
2200.	103.25	96.28
2175.	90.30	95.12
2150.	71.55	93.46
2125.	51.96	84.83
2100.	33.53	78.02
2075.	21.75	66.90
2050.	16.77	57.93
2025.	13.61	36.52
2000.	11.12	11.95
1975.	7.47	6.47
1950.	4.48	6.31

Figure 10. NH_3 #19a, b, and c: Cubic Phase

NOTES

- a) Frost grown by deposition at high flow rate in order to form cubic phase.
- b) NH_3 #19a, b, and c are all the same frost which was held at 77°K and scans were taken at one-hour intervals.
- c) For this frost the flow rate was initially low and when flow was increased the transition to cubic phase was very obvious by visual inspection.

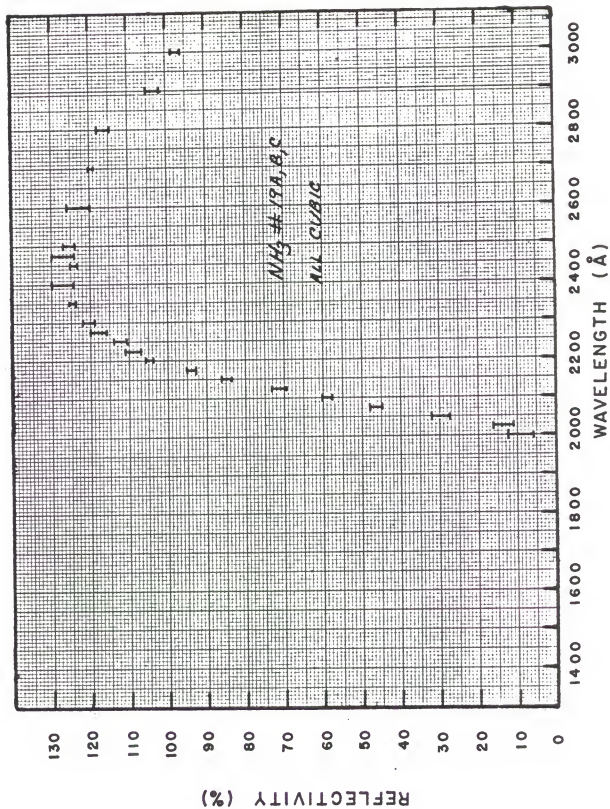


Table 5

-44-

Reflectivity vs. Wavelength for
NH₃ #19a, b, and c

1

WAVELENGTH	NH3 19A	NH3 19B	NH3 19C
3000.	98.43	96.54	98.43
2900.	104.12	102.23	105.54
2800.	115.34	116.92	118.03
2700.	118.50	118.18	120.24
2600.	120.55	122.61	126.24
2500.	124.35	126.08	127.35
2475.	0.0	124.98	130.03
2450.	125.45	124.03	0.0
2425.	0.0	0.0	0.0
2400.	126.24	125.77	130.67
2375.	124.03	0.0	0.0
2350.	124.50	125.29	0.0
2325.	123.71	0.0	0.0
2300.	120.24	119.61	122.45
2275.	116.92	115.97	120.71
2250.	114.71	111.71	112.34
2225.	110.13	106.97	110.60
2200.	105.54	104.75	105.54
2175.	94.48	93.69	95.59
2150.	85.16	86.11	84.85
2125.	71.26	69.99	73.79
2100.	58.78	60.04	58.93
2075.	45.98	46.61	48.19
2050.	29.23	28.12	31.76
2025.	10.90	14.22	15.96
2000.	6.48	10.74	12.48
1975.	5.85	9.95	11.85
1950.	2.05	10.43	12.48

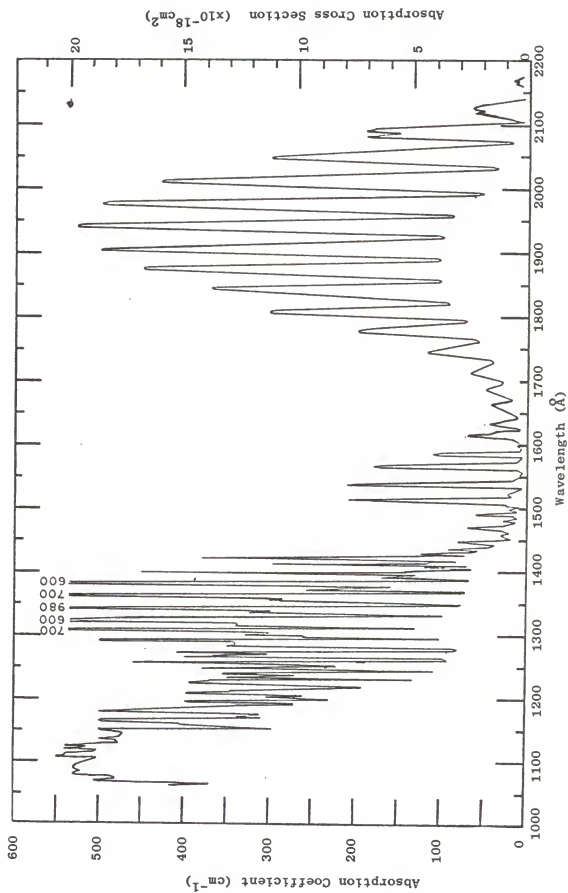


Figure 11. NH_3 Gas Absorption Coefficients (from Watanabe et al., 1953)

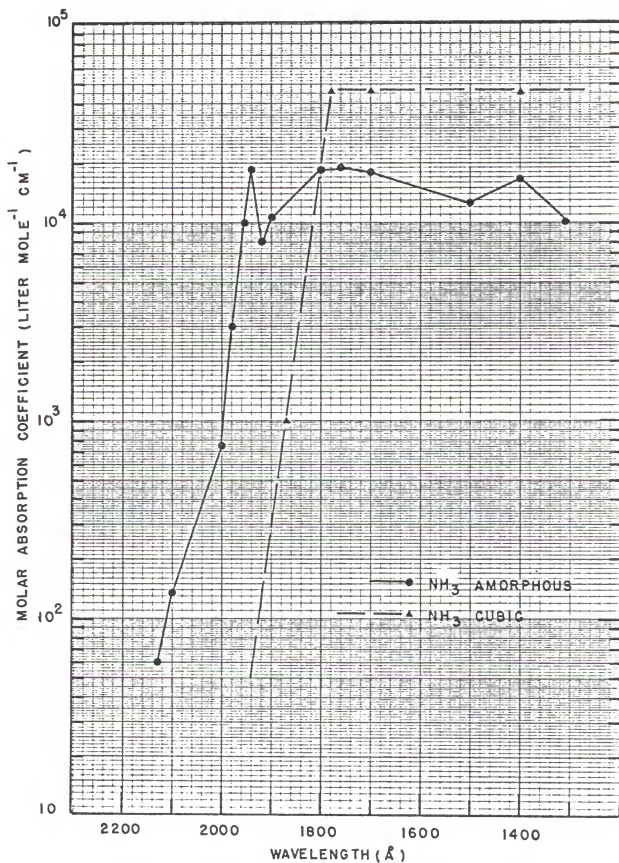


Figure 12. NH₃ Solid Absorption Coefficients (from Dressler and Schnepp, 1960)

Figure 13. Photographs of Cubic and Amorphous NH_3

- A) Amorphous Phase: Note the fine-grain size and matty appearance.
- B) Amorphous Phase: Note the two small pimples in lower right of photo. These are believed to be cubic NH_3 forming on the amorphous NH_3 .
- C) Cubic NH_3 : This cubic phase obtained by rapid deposition at $\sim 180^\circ \text{K}$. The crystals can be seen as white specks.
- D) Same as Photo C. Presented to show large grain size compared to the amorphous.



A



B



C



D

Figure 14. Photographs of NH_3 Frosts Having Various Textures

- A) What was believed to be an amorphous frost with cubic growth overlaying. Note how much brighter the pimples of cubic appear.
- B) An NH_3 cubic frost after annealing at 180°K . Note icy appearance.
- C) NH_3 cubic frost showing large grains.
- D) NH_3 cubic formed by annealing a cubic NH_3 frost similar to that shown in Photo C. Note how annealing greatly reduces the voids between the grains.



A



B

C



D



repeatedly annealed and photometric data recorded after each annealing, e.g., H_2O #13 and 14. Each figure caption gives pertinent information to that particular frost. Reflectivity values are also listed in tabular form; where zeros appear in the tables no data were taken.

Photographs of selected H_2O frosts are shown in Figures 26, 27, and 28 with captions giving the important details. All photographs are twice the actual size. Since the frosts grown with no buffer gas were difficult to photograph most of the photographs are of buffer-gas-frosts. The latter showed substantial structure best described as a ball or "cauliflower" appearance while frosts grown without a buffer gas photographed as uniform white reflectors and little or no structure could be seen in the final prints.

For comparison, the absorption coefficients of H_2O vapor (Watanabe et al., 1953) and H_2O hexagonal and amorphous solids (Dressler and Schnepf, 1960) are reproduced in Figures 23 and 24.

A number of unexpected results were obtained from the H_2O frosts. Most important of these are the absorption features centered at 2200\AA , 2075\AA , and 1925\AA . These features are more pronounced in the cubic H_2O frosts but also appear in some of the amorphous frost reflectivities, e.g., H_2O #14. Since it was anticipated that both NH_3 and H_2O would absorb in a continuum fashion there was immediate speculation that the three absorption features were a result of an unknown contaminant. As reviewed in Appendix 4, the technique for preparing the water was examined in detail and several alternate methods of preparation were employed. Results were always the same, i.e., the absorption features appeared in each H_2O cubic frost.

Next, attention was directed to the photometry but the features in question did not appear in the reflectance measurements of BaSO_4 which was measured out to 1800\AA (see Figure 25). It was thus concluded that the photometry was correct.

The absorption at 1925\AA shows the greatest half width, about 100\AA , and is also characteristic of the manner in which the NH_3 frost absorbed in the cutoff region. Since the majority of the NH_3 experiments preceded the H_2O experiments it was suggested that the NH_3 had been adsorbed by the aluminum flanges of the frost chamber and subsequently outgassed during the H_2O frost growth.

To eliminate this possibility the vacuum chamber was baked out and a 10^{-6} torr vacuum held in the chamber for several days. During the next H_2O experiment (H_2O #13) an amorphous frost was grown, data were taken, and then the frost was annealed above 160°K to obtain the cubic H_2O (this was standard procedure). The reflectance measurements of the cubic H_2O were recorded and the annealing procedure repeated once again. Finally a known amount of NH_3 was deposited on top of the H_2O frost. The result, shown in Figure 19, was an increase in reflectance in the 1925\AA absorption. The amount of NH_3 admitted was approximately fifty times that calculated to be present as a contaminant.

Although this test of NH_3 contamination seemed to indicate that NH_3 was not causing the absorption features in the H_2O frosts, the possibility still existed that the contaminant causing the features could only be influential if embedded with the lattice structure of the H_2O crystals. This reasoning led directly to the theory of solid

state physics and the phenomena of exciton absorption.

Before examining the possibility of explaining the H_2O frost absorption features with exciton theory, several other interesting results from the H_2O frost experiments are discussed.

As was observed for the NH_3 frosts the reflectivity of the H_2O cubic frosts increased from 3000\AA toward shorter wavelengths and in most cases exceeded 100 percent. The reasoning behind this result is identical to that given in the discussion of the NH_3 frost data and thus will not be discussed further.

H_2O #5 and 7 were frosts grown within a closed chamber and thus had a buffer gas present during formation. For #5 the buffer gas (N_2) background pressure was about $10 \mu \text{ Hg}$ and for #7 about $100 \mu \text{ Hg}$. Both of these frosts exhibited the growth of balls ranging in sizes from $< 1\text{mm}$ to about 8mm in diameter. The effect of a buffer gas is not only to increase the growth rate of those frost grains protruding from the surface but also to increase the conductive heat load from the chamber walls. It is clear from Figure 26 that the growing balls have small heat transfer paths to the substrate and this, coupled with the increased conductive heat load, fixed the temperature at the growth sites above the range for amorphous H_2O . Accordingly, both traces shown in Figures 15 and 16 are the reflectivities of cubic H_2O even though the substrate temperature was 77°K . In Figure 15 the trace labeled cubic (a) was the first scan of the "ball" frost and the cubic (b) trace was taken after annealing the frost at temperatures up to 225°K .

Thus, the result of a buffer gas is to mix the amorphous and cubic phases and in most instances grow a cubic H_2O frost overlying an amorphous H_2O . From Figures 15 and 16 it is also clear that since annealing of the buffer-gas-frosts increases the grain size, the shape of the absorption feature at 1925\AA is related to the grain size of the material. No means were available to determine an average grain size during the experiments so at best it can be concluded that an increased grain dimension also increases the strength and width of the absorption features. This grain size effect was also observed by Kieffer (1968) in the infrared region for CO_2 and H_2O frosts.

For H_2O , #10, 12, 13, and 14 the six-inch diffusion pump was open to the frost chamber during the growth period so that the amorphous H_2O was easily formed since all noncondensable (buffer) gases are pumped from the chamber. The amorphous H_2O appeared grey and very fine-grained. It was difficult to obtain an optically thick amorphous frost since this phase of solid H_2O usually grew as a translucent ice. The reflectivity was checked intermittently at 3000\AA during the growth period and when it converged toward the BaSO_4 reflectivity the growth was stopped. Typical growth periods ranged from three to five hours.

The annealing procedure outlined previously was employed to change the amorphous phase to the cubic phase. The H_2O phase change occurred at 150°K and was accompanied by a rise in chamber pressure (see Figure 29). A temperature rise, of the substrate, at the phase change requires an exothermic reaction within the frost. It thus follows that the energy level of the amorphous H_2O must be greater, for a given temperature, than the energy level of the cubic H_2O for a release of heat to occur during the phase change. This further

implies that the vapor pressure of amorphous H_2O should be greater than that of cubic H_2O for a given temperature. When the pressure jump was observed, at the $150^{\circ} K$ phase change, it was felt that this could have been a result of the difference in vapor pressures for amorphous and cubic H_2O . Unfortunately, different vapor pressures could not be positively established for the following reasons:

- a) The vapor pressure for the H_2O cubic has been assumed to be the same as for H_2O hexagonal ice. The vapor pressure of H_2O hexagonal ice has been well established (vapor pressure data taken from the Handbook of Chemistry and Physics, 44th Ed.). This assumption can be in error.
- b) The vapor pressure of the H_2O cubic is $\sim 6 \times 10^{-8}$ torr at $150^{\circ} K$ while the outgassing of the frost chamber, when closed, increased the chamber pressure to $\sim 10^{-3}$ torr in the same time required to warm the frost from $77^{\circ} K$ to $150^{\circ} K$. Consequently, the H_2O pressure measured with the Baratron during the frost warm-up is an unknown partial pressure over the background pressure caused by outgassing and thus the H_2O vapor pressure is only approximately determinable.
- c) During the growth period some noncondensable gas is always trapped within the frost. When the amorphous H_2O molecules reorient and migrate during the change to an ordered structure (cubic phase) the trapped gas is released. This is probably the best explanation of the rise in chamber pressure during the phase change.

Once the cubic H_2O was well established by annealing, the frost was recooled to $77^{\circ} K$ and during this cool-down the diffusion pump was opened to the chamber after the pressure had been reduced to $\sim 500 \mu Hg$ by refreezing of H_2O vapor. The refreezing was somewhat of a problem since it could cause a growth of very fine grains overlaying

the annealed-large-grain frost. The pumping of vapors from the chamber during the recooling of the frost was done to minimize this problem.

For those H₂O frosts grown following the above techniques the amorphous H₂O reflectivities are consistently lower than the cubic H₂O reflectivities (see Figures 17, 18, 19, and 20). The cubic H₂O reflectivities increase 15 to 20 percent from 3000⁰Å to 2400⁰Å. This increase in reflectivity nicely fits a $\lambda^{-0.6}$ law. As discussed by Van de Hulst (1957) the scattering by large spherical particles is explained by a $\lambda^{-\alpha}$ law with $\alpha \leq 1.0$. For $\alpha = 0.6$ the monodispersed particle size is found to be $\sim 1 \mu$. Since the frost particles are not spherical and little is known of the change in complex index of refraction with wavelength for cubic H₂O, the $\lambda^{-0.6}$ law is only illustrative.

No consistent reason can be found to explain the reflectivity of the amorphous H₂O frosts. This is expected since the opacity, grain configuration, and optical constants for the amorphous phase are poorly understood. The physical characteristics of the amorphous phase for both NH₃ and H₂O clearly warrants future attention.

The effects of annealing the H₂O frosts were studied in H₂O #14 (Figure 21). The results show a decrease in reflectivity shortward of 2500⁰Å after each annealing. The cutoff at 1800⁰Å is also influenced, i.e., the annealed frosts have lower reflectivities between 1800⁰Å and 1700⁰Å.

The possibility of attributing the absorption features at 2200⁰Å, 2075⁰Å, 1925⁰Å to a photon-exciton interaction can only be discussed in general terms since (to the knowledge of the author) experimental research, into the physics of solid water, is inconclusive at the

present time. The initial suggestion that exciton absorption is causing the structure in the reflectivity of solid H_2O observed in this work was made by Prinz (1972). An excellent review of exciton theory is given by Knox (1963).

The first explanation of absorption features in perfect insulating materials was given by Frankel, Peierls, and Wannier (ref. Knox, 1963) in the early 1930's. Since that time, exciton-phonon-photon interaction has been established and many elements and organic compounds studied. The most simplified exciton energy state model is the hydrogen-like model and is similar to the Rydberg series.

The features observed in the H_2O frost were reviewed in light of the hydrogenic type series and no definite conclusion can be made at this time.

Figure 15. H_2O #5a and b: Cubic Phase

NOTES

- a) This frost was grown with a $10\ \mu$ Hg buffer gas (N_2).
- b) Both traces are cubic H_2O . Trace "b" is after frost was annealed at $T \sim 225^\circ\text{K}$ for about one-half hour.

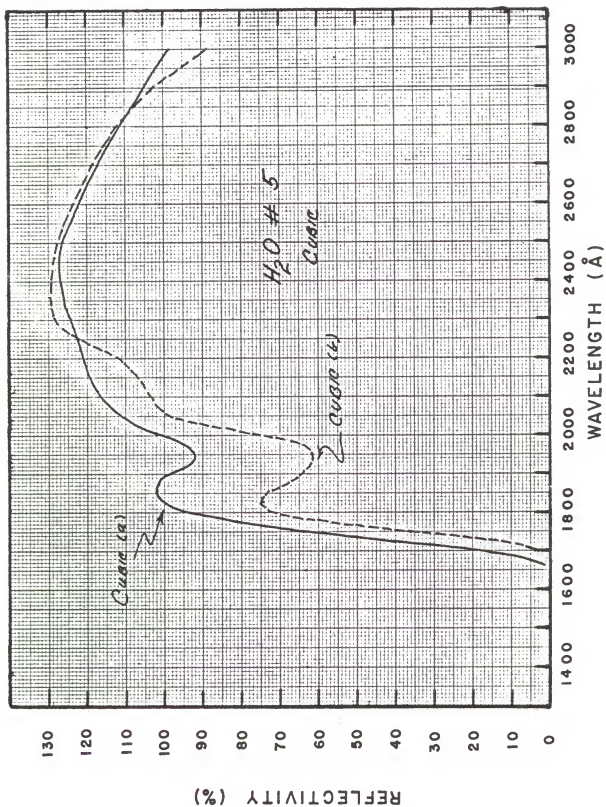


Table 6

-60-

Reflectivity vs. Wavelength for
H₂O #5a and b

WAVELENGTH	HOH 5A	HOH 5B
3000.	98.79	89.89
2900.	106.62	103.77
2800.	120.86	113.03
2700.	117.48	119.97
2600.	121.93	121.40
2500.	127.98	128.69
2400.	126.74	129.05
2300.	124.07	129.41
2250.	0.0	0.0
2200.	122.11	111.61
2150.	119.08	0.0
2100.	117.48	104.31
2075.	0.0	0.0
2050.	0.0	100.57
2025.	0.0	77.43
2000.	102.53	77.25
1975.	0.0	0.0
1950.	92.56	62.83
1925.	0.0	0.0
1900.	99.50	64.97
1875.	97.19	67.64
1850.	102.71	73.34
1825.	98.26	75.12
1800.	95.41	73.34
1775.	80.10	59.63
1750.	64.26	37.74
1725.	40.23	14.06
1700.	17.62	3.38

Figure 16. H_2O #7a and b: Cubic Phase

NOTES

- a) This frost was grown with a $10\ \mu$ Hg buffer gas (N_2).
- b) Both traces are cubic H_2O . Trace "b" is after annealing for one and one-half hours at $T = 225^\circ K$. Note the increased difference in reflectivity of trace a and b with annealing time. In H_2O #5 the annealing was done for about one-half hour.

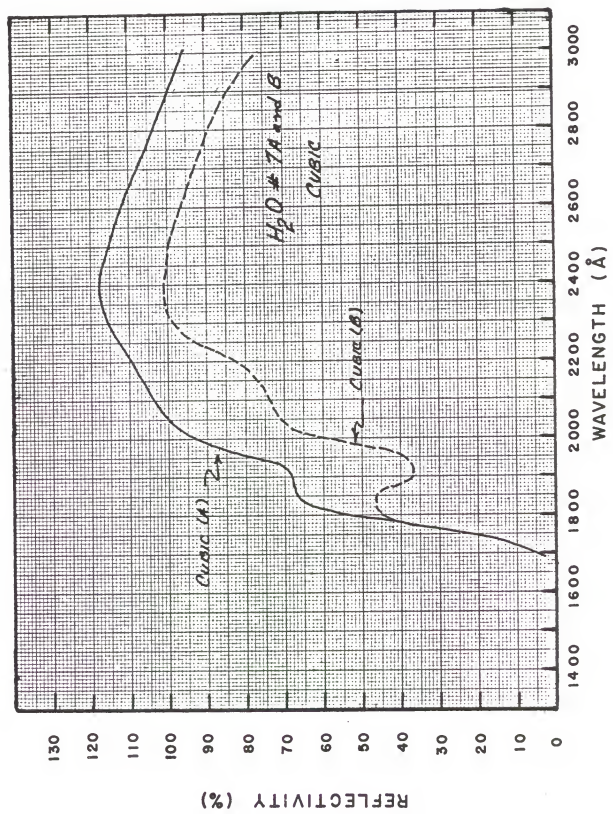


Table 7

-63-

Reflectivity vs. Wavelength for
H₂O #7a and b

WAVELENGTH	HOH 7A	HOH 7B
3000.	97.01	76.18
2900.	98.43	87.22
2800.	108.58	87.04
2700.	106.27	95.76
2600.	113.39	96.30
2500.	115.34	101.46
2400.	119.97	100.21
2300.	114.45	100.93
2250.	0.0	94.34
2200.	112.67	83.66
2150.	106.27	77.25
2100.	104.66	74.23
2075.	0.0	73.69
2050.	100.21	71.02
2025.	102.17	68.71
2000.	93.63	58.56
1975.	87.93	47.53
1950.	74.76	39.87
1925.	75.83	38.09
1900.	68.71	37.38
1875.	68.17	42.01
1850.	67.64	46.99
1825.	63.55	40.76
1800.	54.29	45.57
1775.	36.67	36.49
1750.	19.22	24.92
1725.	10.15	13.35
1700.	4.63	5.52

Figure 17. H O #10: (a), Amorphous Phase; (b), Cubic Phase

NOTES

- a) Trace (a) is very fine-grained amorphous H_2O .
- b) Trace (b) is cubic frost annealed from amorphous frost.
- c) The amorphous frost in this experiment may not have been optically thick. The frost was grown to examine the absorption features at 2200\AA , 2075\AA , and 1925\AA .
- d) Chamber was closed.
- e) No buffer gas.
- f) Amorphous growth period was 1.5 hours.
- g) The $\lambda^{-.6}$ law is shown by triangles for $\lambda > 2200\text{\AA}$.

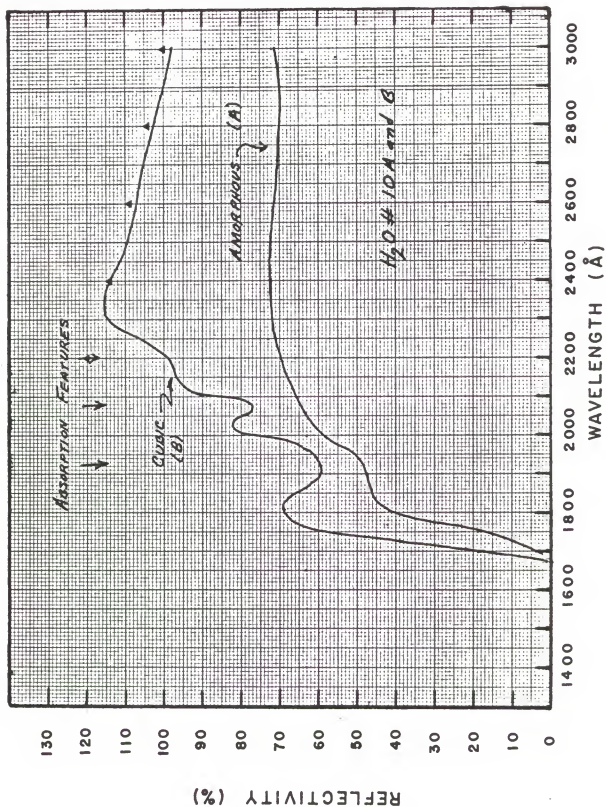


Table 8

=66=

Reflectivity vs. Wavelength for
H₂O #10a and b

WAVELENGTH	HOH 10A	HOH 10B
3000.	72.20	98.17
2900.	69.91	101.23
2800.	72.01	103.52
2700.	70.86	108.49
2600.	72.01	109.82
2500.	73.53	109.63
2400.	72.58	114.98
2300.	72.01	115.36
2250.	73.34	106.39
2200.	66.09	99.32
2150.	68.57	97.60
2100.	65.51	91.49
2075.	70.10	77.55
2050.	63.98	78.31
2025.	62.27	82.51
2000.	63.22	74.30
1975.	56.73	64.37
1950.	50.42	62.65
1925.	48.70	61.31
1900.	49.47	59.78
1875.	47.94	63.22
1850.	46.60	67.61
1825.	46.22	68.57
1800.	41.06	70.48
1775.	32.28	65.51
1750.	18.14	56.34
1725.	10.70	40.87
1700.	4.77	17.57

Figure 18. H_2O #12: (a), Amorphous Phase; (b), Cubic Phase

NOTES

- a) Frost growth and annealing the same as H_2O #10.
- b) The same procedures were followed as in H_2O #10 to establish the repeatability of observing the absorption features.
- c) The absorption features were seen in the H_2O amorphous. This may indicate that some cubic structure was present.

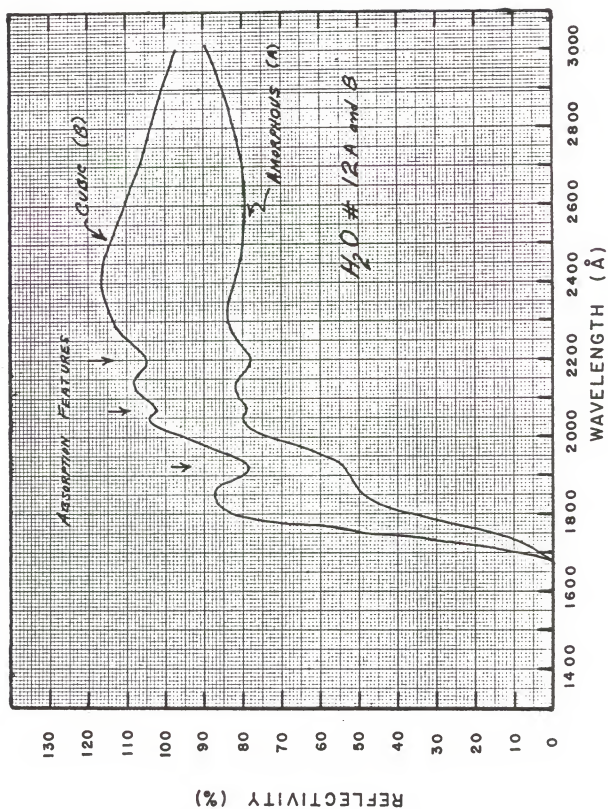


Table 9

Wavelength vs. Reflectivity for
H₂O #12a and b

WAVELENGTH	HOH 12A	HOH 12B
3000.	84.45	97.52
2900.	91.16	102.86
2800.	84.62	104.75
2700.	80.67	106.30
2600.	80.15	111.97
2500.	80.32	114.21
2400.	82.56	117.48
2300.	84.62	113.69
2250.	82.90	112.14
2200.	78.95	105.61
2150.	81.01	108.70
2100.	81.18	105.61
2075.	79.46	102.68
2050.	80.15	104.58
2025.	77.92	96.84
2000.	75.51	96.84
1975.	66.05	89.78
1950.	60.37	84.28
1925.	54.70	78.09
1900.	52.63	85.31
1875.	50.22	85.83
1850.	48.16	88.41
1825.	44.03	86.52
1800.	37.15	83.76
1775.	26.66	68.97
1750.	16.86	48.16
1725.	8.43	23.56
1700.	4.13	7.57

Figure 19. H₂O #13A: Amorphous Phase

NOTES

- a) This frost grown to examine absorption features in the cubic phase when NH₃ is added on top of H₂O cubic.
- b) The amorphous frost was grown and reflectivity measured to see if cubic absorption feature would be present. Only the 1925A dip was seen.
- c) Frost grown at very slow flow rate.
- d) Growth period 3.5 hours.

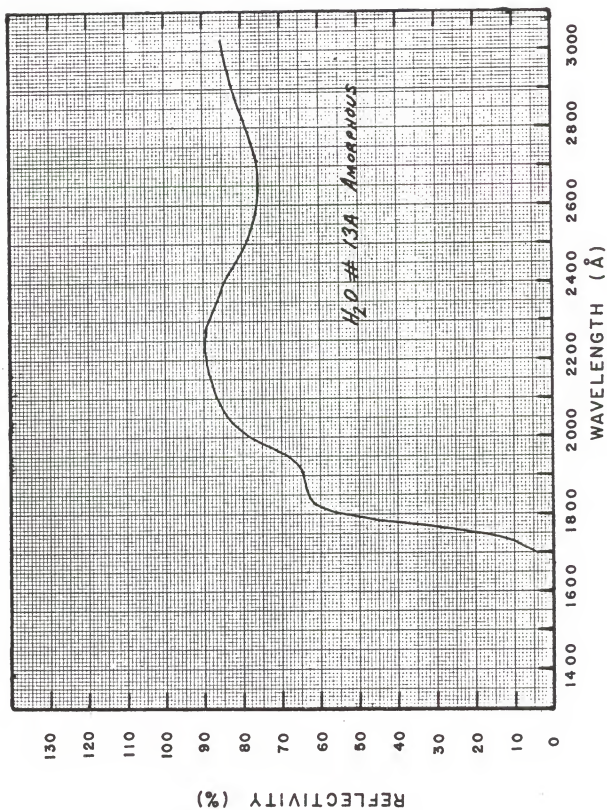


Figure 20. H₂O #13: (b), (c), Cubic Phase; (d), NH₃ Added Over H₂O Cubic

NOTES

- a) Traces (b) and (c) are cubic H₂O. Trace (c) was annealed a second time. Trace (d) is reflectivity of H₂O cubic with a NH₃ concentration of approximately .003 mole/liter. The NH₃ was added on top of H₂O cubic.
- b) Each annealing of frost (b) and (c) was about 45 minutes.
- c) Note the increase in reflectivity when NH₃ was added. This could be explained by an increase in scattering by the fine-grained NH₃ particles formed over coarse H₂O cubic grains.

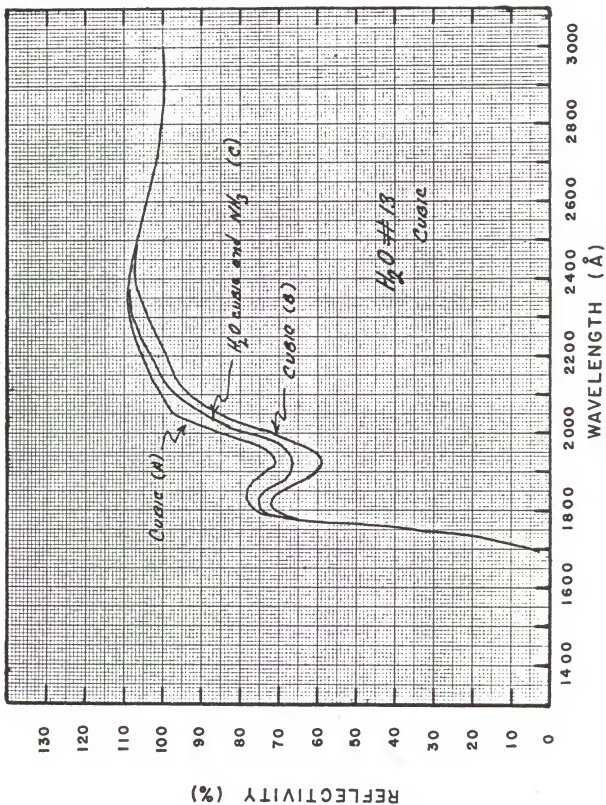


Table 10
 Reflectivity vs. Wavelength for
 H_2O #13 a, b, c, and d

HOH FROST 13

WAVELENGTH	A	B	C	D
3000.	80.49	97.86	99.87	100.87
2900.	83.00	99.87	94.02	101.03
2800.	79.83	100.87	102.54	104.21
2700.	76.49	99.53	0.0	102.04
2600.	76.32	105.21	101.37	106.88
2500.	79.66	100.87	0.0	109.55
2400.	85.67	109.89	108.88	111.22
2300.	89.01	107.88	0.0	110.22
2250.	91.35	107.21	0.0	107.55
2200.	89.34	100.87	99.20	102.04
2150.	88.84	100.87	98.20	101.87
2100.	86.00	100.20	92.18	98.53
2075.	88.18	96.36	91.85	96.36
2050.	84.33	98.20	86.67	90.85
2025.	87.01	90.85	87.51	86.51
2000.	79.49	85.34	74.31	79.83
1975.	75.98	76.32	66.80	70.47
1950.	68.64	73.65	60.45	69.47
1925.	65.46	71.31	60.79	66.47
1900.	64.63	74.31	61.12	68.47
1875.	63.96	74.65	64.13	69.47
1850.	62.12	78.66	70.64	74.15
1825.	62.12	77.32	74.31	75.98
1800.	53.94	76.65	71.31	74.65
1775.	38.91	59.79	59.79	59.45
1750.	19.71	36.07	34.07	36.74
1725.	9.52	14.03	11.02	13.69
1700.	4.68	3.67	3.67	3.51

Figure 21. H₂O #14: (a), Amorphous Phase

NOTES

- a) The amorphous H₂O showed the absorption features as did H₂O #12. Again this is believed to be a result of some cubic H₂O present (possibly overlaying the H₂O amorphous).
- b) Since the reflectivity increased going from 3000^oÅ to 2400^oÅ, this is also evidence of some H₂O cubic present.

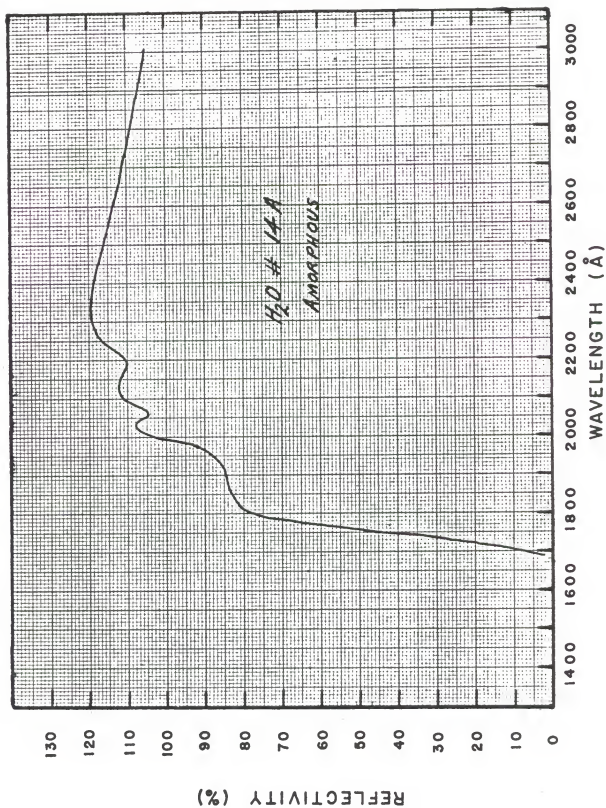


Figure 22. H_2O #14: (b), (c), (d), Cubic Phase

NOTES

- a) This frost was annealed three separate times after being transformed to the cubic phase.
- b) Each annealing was about 45 minutes at $T \sim 225^\circ \text{K}$.
- c) Note the respectable decrease in reflectivity for wavelength between 2100\AA and 2500\AA , after each annealing.
- d) Note also the difference in reflectivity cutoff after each annealing.

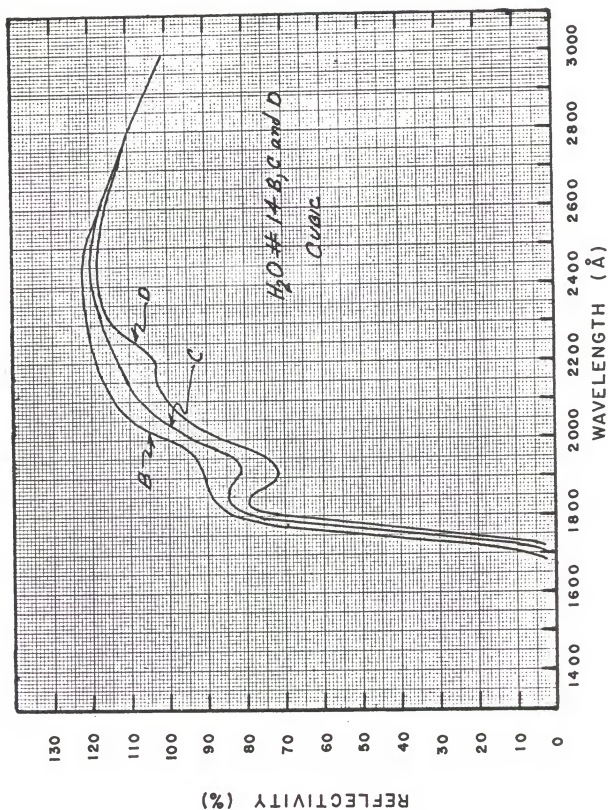


Table 11

Reflectivity vs. Wavelength for
H₂O #14 a, b, c, and d

1

HOH FROST 14

WAVELENGTH	A	B	C	D
3000.	105.72	97.77	102.51	90.42
2900.	109.55	109.85	0.0	94.86
2800.	109.55	108.63	113.83	110.77
2700.	110.92	115.51	0.0	113.07
2600.	115.21	116.59	115.82	116.59
2500.	114.75	122.71	0.0	118.27
2400.	119.34	122.55	120.56	118.73
2300.	119.49	120.41	117.81	115.36
2250.	118.12	121.79	114.14	108.17
2200.	110.62	111.84	112.61	103.73
2150.	112.45	116.74	112.00	104.04
2100.	111.69	115.97	108.48	99.14
2075.	106.03	115.36	104.65	99.91
2050.	104.35	109.39	105.42	96.85
2025.	108.78	106.18	96.08	93.64
2000.	104.50	101.90	94.09	86.14
1975.	92.72	95.47	85.37	82.16
1950.	88.43	93.94	85.68	74.20
1925.	85.22	89.05	80.94	74.51
1900.	84.00	92.72	82.47	72.67
1875.	84.00	89.35	84.15	76.35
1850.	82.31	85.99	84.46	79.10
1825.	84.15	87.36	83.69	79.25
1800.	77.42	83.08	76.81	70.84
1775.	65.18	70.07	58.45	49.57
1750.	43.30	46.66	29.99	23.87
1725.	23.26	20.96	8.11	7.04
1700.	8.41	6.27	3.06	2.75

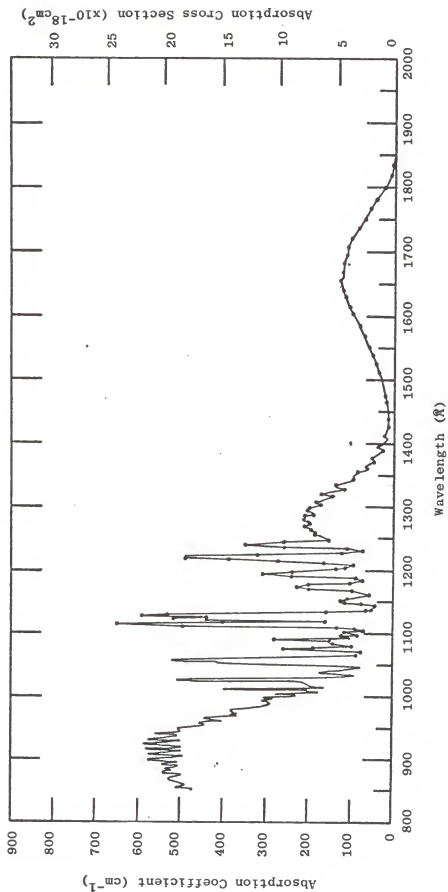


Figure 23. H₂O Vapor Absorption Coefficients (from Watanabe et al., 1953)

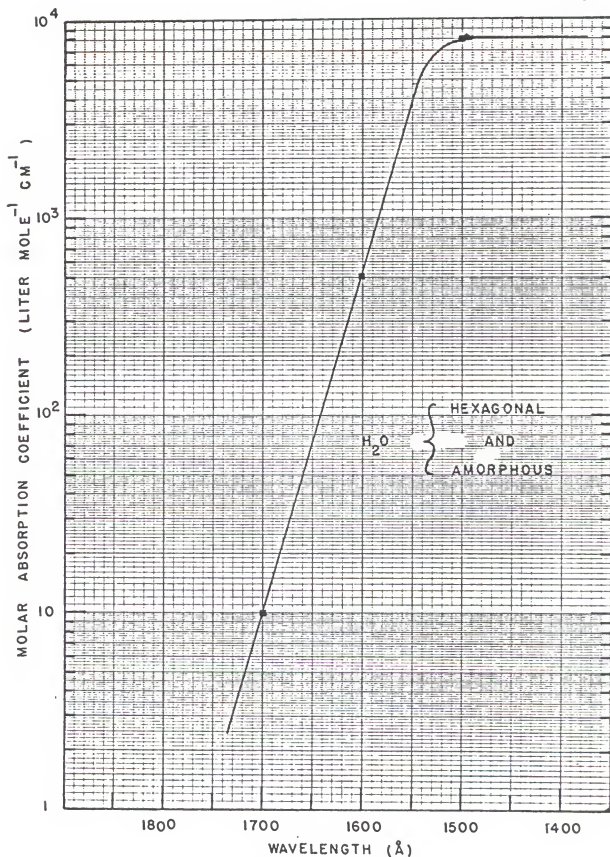


Figure 24. H_2O Solid Hexagonal and Amorphous Absorption Coefficients (from Dressler and Schnepf, 1960).

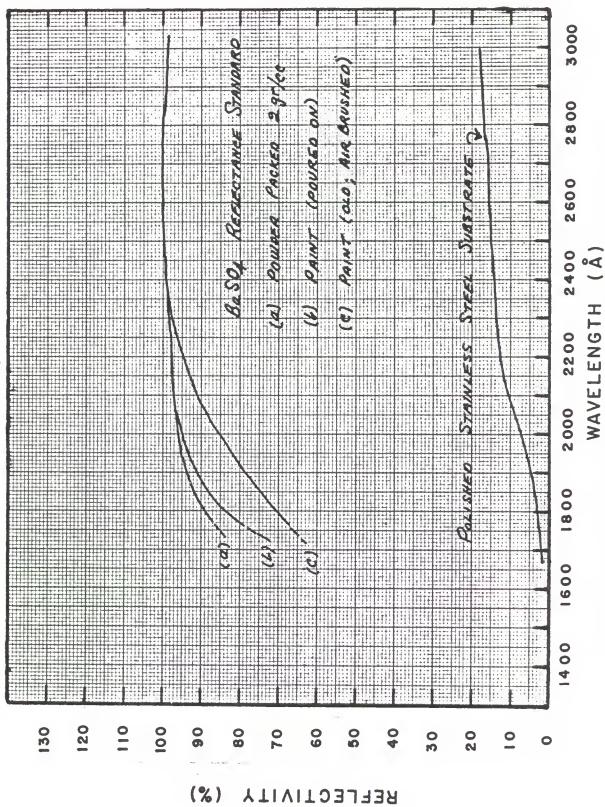
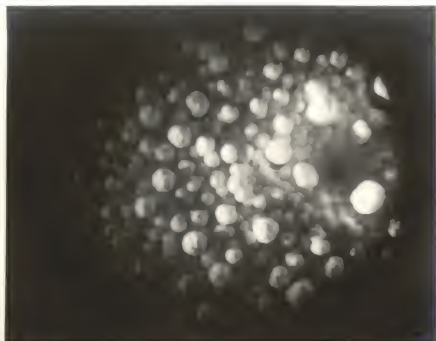
Figure 25. BaSO_4 and Stainless Steel Substrate Reflectivities

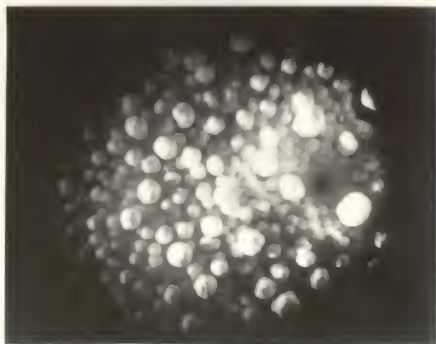
Figure 26. Photographs of H_2O Cubic Frosts
Grown with a Buffer Gas

NOTES

- A) This H_2O frost was grown at a slow rate with a 1000 μ buffer gas (N_2). The vacancy in the center righthand of the photo was once occupied by a "ball." Note the manner in which the small balls were packed around the missing ball of frost.
- B) Same photographs as "A" except for exposure time.



A



B

Figure 27. Photographs of H_2O Buffer-Gas-Frosts
and H_2O Amorphous Frost

NOTES

- A) H_2O frost grown at high deposition rate with buffer gas of $1000 \mu \text{ Hg (N}_2\text{)}$. The "ball" type frost did not develop because of the nonuniform deposition obtained by a high inlet flow of H_2O vapor. This frost is cubic even though deposition took place at 77° K (see text for further discussion).
- B) Same as frost "A"; photo was taken at a different location of dewar.
- C) H_2O amorphous frost. Note the fine-grain size. Although this frost cracked and no photometric data were taken, it depicts the optical thickness of an amorphous frost. The lighting is from the top of the picture and in the crack which protrudes from the dewar it is clear the light penetrates the frost for approximately $1/16$ inch. The small "ball" in this photo is the cubic H_2O forming over the amorphous.
- D) Same frost as in photo "C" but taken earlier in the growth period.



A



B



C



D

Figure 28. H_2O "Ball" Frost Growth Sequence

NOTES

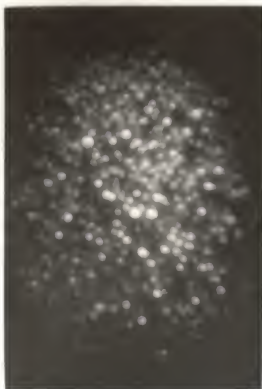
These photographs were taken at 30-minute intervals during the growth period. The buffer gas is N_2 at 500 μ . Note in photograph "A" the underlying amorphous H_2O formed at 77⁰ K during start of flow.



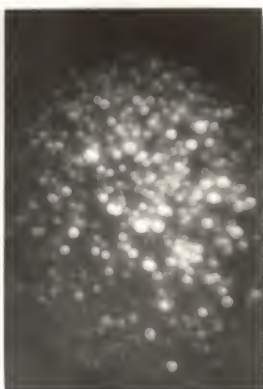
A



B



C



D

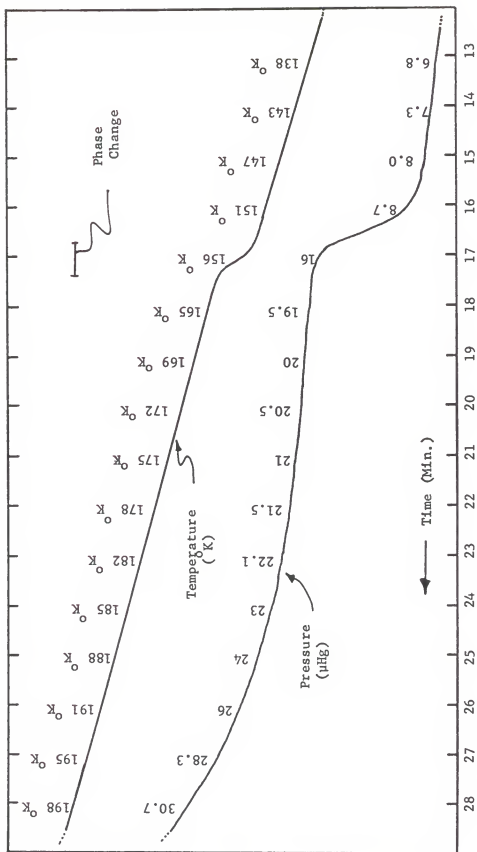


Figure 29. H₂O Phase Change Data (Temperatures, °K, shown are from substrate thermocouple and pressures are from the MKS Baratron transducer in μ Hg).

IV. Conclusions

The reflectivities of NH_3 and H_2O frosts were measured from 3000\AA to 1400\AA and the effects on reflectivity of grain growth, cubic or amorphous phase, and buffer gas were examined.

The reflectivities of the NH_3 frosts are above 90 percent longward of 2300\AA and below 1 percent from 1950\AA to 1400\AA . The absorption cutoff from 2200\AA to 1950\AA occurs at longer wavelengths than those expected from the absorption coefficients of solid NH_3 measured by Dressler and Schnepp (1960).

The H_2O frost reflectivity measurements are quite different from anything anticipated. Based on absorption data of Dressler and Schnepp, a H_2O frost should not become "black" until approximately 1500\AA . The present study shows that if the H_2O frosts are optically thick at 3000\AA the reflectivity will decrease to less than 10 percent between 1800\AA and 1700\AA . This aspect is more important in relation to the study of the Jovian planets, in particular Saturn's rings. Since the solar radiation at 1800\AA is approximately an order of magnitude greater than at 1500\AA , detection of a solid H_2O absorption will be easier than previously thought.

It was also discovered that the H_2O cubic frosts contained absorption features which are not seen in H_2O vapor. The possibility

of these absorptions being caused by excitons was suggested.

The reflectivity of NH_3 #10, a cubic frost, is plotted against the UV albedo of Jupiter (from Anderson et al., 1969) in Figure 30. The Jupiter data were normalized to the frost data at 2400\AA . Wavelength ranges labeled A, B, and C correspond to the first drop in the Jovian albedo from 2200\AA to 2000\AA , to the somewhat level region from 2000\AA to 1800\AA and to the sharp cutoff at 1800\AA , respectively.

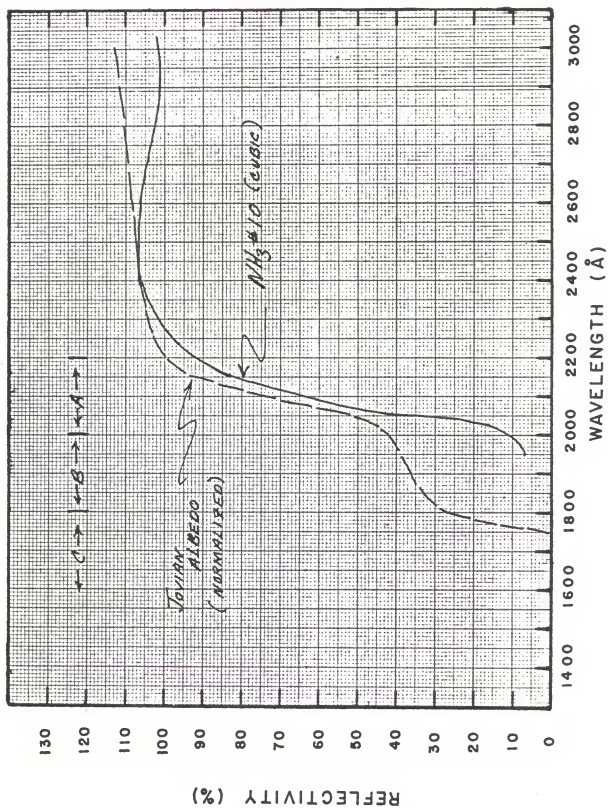
Comparison of the NH_3 frost data with the Jupiter albedo in the three wavelength regions shows good agreement only in the region A. However, as stated by Anderson et al. (1969), region A can also be explained with gaseous NH_3 absorption. The absorption bands of NH_3 gas would not appear in the Jupiter albedo since the resolution of the rocket data was too low. In short, both gaseous and solid NH_3 could explain the Jupiter albedo in the wavelength range A.

It is unfortunate that no frost data could be recorded below 1900\AA . Nevertheless, the frost data between 1900\AA and 2000\AA do have a trend similar to that of the Jupiter albedo.

No comment can be made concerning the wavelength range C. It should be mentioned, however, that the Jupiter albedo cutoff at 1800\AA is very similar to the H_2O frost cutoff.

Finally, no comparison of the H_2O frost data to the albedo of the Saturnian ring can be made at present. The only available Saturnian UV data are that from the OAO-2 (see Wallace et al., 1972) and these data are an integrated ring plus disk albedo.

Figure 30. Comparison of Jovian UV Albedo to NH_3
Frost Reflectivity.



APPENDICES

Appendices Introduction

The intent of the following appendices is to present a detailed description of the instrumentation and procedures employed to measure the UV reflectivities of the NH_3 and H_2O frosts. The creditability of the final results of any experimental research always depends upon the completeness to which the techniques employed are understood.

Some of the procedures and apparatuses established in the design phase of the project were found to contain undesirable aspects after the equipment had been constructed and tested. Some of these difficulties were correctable but more important is that all of the techniques which contained experimental error were recognized.

It is hoped that the following appendices contain sufficient detail to allow an accurate judgment of the reliability of the results.

Appendix 1

Light Source

The design of the light source was centered around the Evenson type microwave cavity (see Fehsenfeld et al., 1964). The cavity was powered by a Scintillonics 2450 MHz microwave generator. The cavity takes a 13mm Quartz tube in which the discharge gas is located. For this source the discharge gas was H_2 at pressures ranging from 1000 μ Hg to 500 μ Hg. The continuum and line flux-output of the light source is shown in Figure 30. For wavelengths short of $1800\overset{\circ}{\text{\AA}}$ it was initially hoped that Kr could be used as the discharge gas since it exhibits a continuum output at these wavelengths. Later it was found that the contamination by H_2 caused the Kr continuum to be swamped by intense lines. This presented no problem since the H_2O and NH_3 frosts were strongly absorbing short of $2000\overset{\circ}{\text{\AA}}$ and the intense lines of the H_2 discharge were exactly what was needed in order to record any reflected radiation.

The discharge tube was continuously fed with laboratory grade H_2 through a Veeco variable leak valve and pumped by a mechanical vacuum pump. Some contamination by N_2 was always present and resulted in a series of lines between $3400\overset{\circ}{\text{\AA}}$ and $2900\overset{\circ}{\text{\AA}}$ as shown in Figure 30. When the frost data were taken some readjustment of the monochromator

slits was required for $2900\text{\AA} < \lambda < 3400\text{\AA}$ but from 2900\AA to about 1680\AA the H_2 continuum output proved to be very convenient.

The Evenson cavity could be "dead tuned" by adjustment of a coupling slider and a tuning stub. The reflected and forward power was measured by a power meter in the Scintillonics power supply and when the voltage standing wave ratio (VSWR) was approximately ten the discharge was ignited by a Tesla coil. Some readjustment of the cavity was required after the discharge was active. Later in the experiment period it was found that the cavity could be left tuned for the active discharge and still be started with the Tesla. The discharge ran at a typical input power of 70 watts. The VSWR was reduced to almost unity by careful tuning.

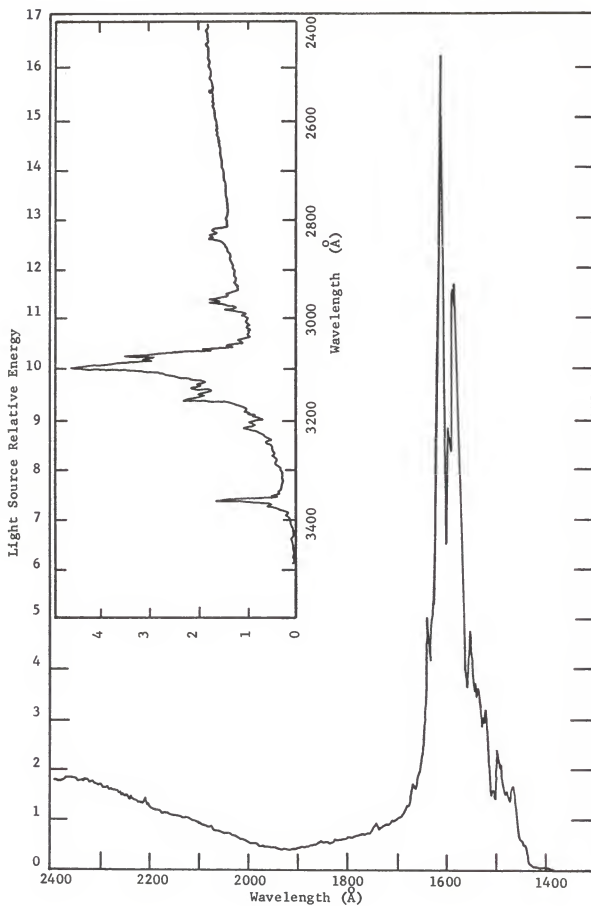
The light source was positioned as close to the entrance slit of the monochromator as possible and was separated from the monochromator by a 1mm thick, 1/2" diameter MgF_2 window. This MgF_2 window had to be cleaned from time to time, however, the light source was used for approximately fifty hours and the MgF_2 window seems to have lost little transmissivity.

Overall the light source performed very satisfactorily throughout the experimental period.

Figure 31. H_2 Light Source Output as a Function
of Wavelength

NOTES

- a) The insert shows the light source output from 3400 \AA and the main figure shows the output from 2400 \AA to 1400 \AA .
- b) Monochromator slits were 200 μ x 200 μ .
- c) PM 9553 recorded the output. High voltage was 2800 volts.
- d) H_2 discharge pressure was 350 μ .
- e) Microwave generator was set at 70 watts forward power. The VSWR was 1.2.

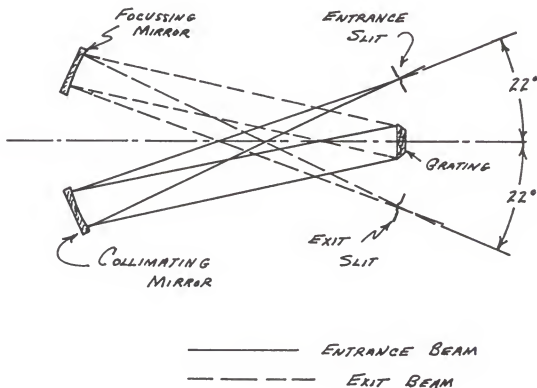


Appendix 2

Monochromator

The monochromator was purchased commercially from the McPherson Instrument Corporation, Model 218. Features of this model are the following:

- 1) .3 meter focal length.
- 2) 1200 grooves per mm snap-in type grating.
- 3) high speed F/5.3 exit beam.
- 4) operational to 1000\AA when evacuated.
- 5) independently adjustable slits.
- 6) resolution capability $.6\text{\AA}$.
- 7) scans to "o"-order.
- 8) optical arrangement shown below.



The McPherson was evacuated to 10^{-6} torr with a 2" Chevron cryo-baffle and a 2" oil diffusion pump backed by a 15 cfm Duo-Seal forepump. The forepump and diffusion pump were separated by a Veeco coaxial foreline trap to prevent forepump oil from backstreaming into the monochromator. A 2" air operated gate valve separated the McPherson from the vacuum pump, and was controlled by a safety electrical shutdown circuit. This combination was arranged such that in the event of a power failure the gate valve would close and the diffusion pump would automatically shut off.

Scattered light from the McPherson was checked by monitoring the output radiation with a solar-blind photomultiplier tube (PM tube) while scanning the monochromator to wavelengths outside the range of radiant sensitivity of the PM tube. Some signal could be seen below 1400\AA if the PM tube gain was at a maximum setting and if the exit and entrance slits of the monochromator were set to $2000\text{ }\mu \times 2000\text{ }\mu$ (the maximum opening of the slits). However, the slits were usually $800\text{ }\mu \times 800\text{ }\mu$ during the frost experiments. At this setting the scattered light for $\lambda < 1400\text{\AA}$ was never above 5 percent of the light output for $1400 < \lambda < 3400\text{\AA}$. It is felt that if the PM tubes could have been more solar-blind, for example the rubidium telluride photocathode long wavelength cutoff is 3200\AA while the PM tubes used herein were cesium telluride with a long wavelength cutoff at 3400\AA , the scattered light component would have been essentially zero.

Appendix 3

Frost Chamber

The basic layout of the 6" Pyrex cross used for a frost chamber has been given in the main text and only a few additional points need to be made.

The chamber outgassing rate was measured by closing the 6" gate valve and recording the rise in chamber pressure with the MKS Baratron. The chamber would come to about 4μ Hg in one hour starting from 10^{-6} torr. This high outgassing rate was due to the necessary instrumentation located inside. Even though all PM tube wires were Teflon insulated and no materials other than metals were used inside the chamber, the outgassing could not be further reduced. The chamber was leak-tested with a He leak detector and no leaks were found. It was concluded that outgassing was at fault. It was hoped that the outgassed constituents were noncondensable at 77° K and were removed by keeping the chamber open to the vacuum pumps during the frost growth period.

An important component of the frost chamber was the aluminum cold shield labeled part "J" in Figure 1. The shield was an aluminum tube 5 1/2" in diameter and was attached to the frost dewar. Thermocouple measurements at the front of the tube indicated that the tube was cooled to $\sim 100^{\circ}$ K while closer to the dewar the temperature was even lower. This shield served to carry a large portion of the thermal

conduction heat load from the chamber walls and thus the frost was exposed to "wall temperatures" of 100° K instead of 300° K. The shield also served to keep any frost fragments from falling into the vacuum pump and to attach several additional components, e.g., the BaSO_4 reference and an observation light.

Components of the vacuum system employed to pump the frost chamber were the following:

- a) Six-inch oil diffusion pumps manufactured by Norton Vacuum Equipment Division. The oil used was DC-705.
- b) Six-inch Chevron Cryo-Baffle was the cold trap for the diffusion pump.
- c) An air-operated 6" gate valve separated the diffusion pump and cold trap from the frost chamber. This gate valve was controlled by the power failure safety-shutoff system which also controlled the gate valve on the monochromator vacuum system.
- d) The diffusion pump was backed by a 15 cfm Duo-Seal mechanical vacuum pump. This same pump was connected via vacuum valves to the diffusion pump for the McPherson monochromator.

The vacuum grease used on all parts was Apiezon L.

Appendix 4

Source Gases

The NH_3 gas was purchased commercially from Air Products and Chemicals, Inc. The ultra high pure (UHP) grade NH_3 was of acceptable purity (99.999 percent). It must be remembered, however, that if the frost chamber were filled to a pressure of one atmosphere with the UHP NH_3 and then the frost dewar cooled to 77°K , the residual pressure, after all the NH_3 had frozen out, would be roughly $7.6 \mu \text{Hg}$. During a frost growth the quantity of NH_3 consumed is estimated to have been between twenty and fifty times the chamber volume (STP). Clearly if the chamber is closed during the frost growth period the background pressure would become substantial. For this reason the chamber was left open to the vacuum pump throughout the growth period.

Perfection of the techniques needed to obtain pure H_2O vapor required some months' trial and error.

The first H_2O system attempted was to collect a sizable volume of distilled water in a reservoir and if this supply were found to be of an acceptable purity no further distillation would be required. This approach was soon found to be completely inadequate. The water was in constant contact with the aluminum flanges of the reservoir and no means were available to check the water purity once the reservoir had been filled.

After a number of minor alterations the most favorable procedure was the following: 1) a small glass vacuum trap was employed to collect the distilled water. This trap was cleaned with chromic acid and continuously leached with conductivity water taken directly from the still. 2) The conductivity of the water was checked with a Leeds and Northrup conductivity meter until the acceptable limit of ion concentration was reached. 3) This conductivity water was immediately connected to the frost chamber inlet line and to an evacuation line. While the water was still hot a vacuum was slowly drawn on the glass reservoir until the water just began to boil. This vacuum boiling removed almost all of the N_2 absorbed in the water. 4) Each H_2O frost was grown from a new batch of conductivity water.

By specifying the acceptable water purity at a conductivity of $.5 \times 10^{-6} \text{ ohm}^{-1} \text{ cm}^{-1}$ the concentration of contaminants can readily be calculated. It is commonly known that ammonia is the most difficult contaminant to remove from water and since the most pronounced absorption feature in the H_2O frosts resembled the NH_3 cutoff spectrum it was assumed NH_3 was the contaminant of greatest concern.

In the field of electrochemistry it was first established by Arrhenius that the percentage of ionic dissociation rapidly increases with decreasing concentration. The concentrations of NH_3 dealt with in this study were very small and it seemed safe to assume that the NH_3 was entirely dissociated into NH_4^+ and OH^- ions. A measurement of the NH_4^+ ion concentration is thus a direct measure of the NH_3 concentration in the H_2O vapor contained in the reservoir.

To determine the concentration of NH_4^+ the equivalent conductivity is first defined, i.e.,

$$\Lambda = K/C$$

where Λ is the equivalent conductivity [$\text{ohm}^{-1} \text{cm}^2 \text{equivalents}^{-1}$], K is the specific conductivity [$\text{ohm}^{-1} \text{cm}^{-1}$] and C is the concentration [equivalents cm^{-3}]. The concentration is measured in equivalents, where one equivalent is the weight of substance necessary to give one mole of H or OH in a neutralization reaction. Put another way, the equivalence is the formula weight divided by the valence. For example, if the ions that neutralize a one molar solution of H^+ have a valence of two then only .5 moles need be added. If the valence is unity the concentration is in equivalents per liter or simply moles per liter.

For large concentrations of NH_4OH the equivalent conductivity is listed in the Handbook of Chemistry and Physics. The values are:

Λ	\sqrt{C}
238.00	0.0000
9.66	0.1000
5.66	0.1732
3.10	0.3160

Since NH_4OH is a weak electrolyte the equivalent conductivity increases very rapidly for dilute mixtures. To calculate C a conservative estimate of 100 for Λ is taken and the specific conductivity was experimentally measured to be $.5 \times 10^{-6} \text{ohm}^{-1} \text{cm}^{-1}$. Thus $C = K/\Lambda = 5. \times 10^{-9}$ equivalents per liter or moles per liter. For NH_4OH there are 35 grams per mole so $C \approx .2 \times 10^{-6} \text{gr/cc}$.

For a concentration of .2 ppm of NH_3 it is highly unlikely that any feature in the H_2O frosts could be caused by NH_3 .

It was thus concluded that the absorption features observed in the H_2O frosts were indeed due to absorption by water molecules or as suggested by excitons.

The equilibrium vapor pressures for NH_3 and H_2O were calculated for temperatures below those for which empirical data are available by the following equation:

$$\log_{10} P = -\frac{a}{T} + b$$

where T is the absolute temperature, P is the pressure in mmHg and a and b are constants.

This equation was fitted to the empirical data and then the vapor pressures were calculated for temperature down to 77°K . The final form of the vapor pressure-temperature relationships for NH_3 and H_2O were:

$$\text{NH}_3: \quad \log_{10} P = \frac{-16.302 \times 10^2}{T} + 9.9974$$

$$\text{H}_2\text{O}: \quad \log_{10} P = \frac{-26.660 \times 10^2}{T} + 10.5510.$$

Appendix 5

Calibration of PM Tubes

The total errors in the reflectivity measurements are due to the uncertainties in the cross-calibration of the PM tubes used to measure the incident and reflected radiation. No two photoelectric detectors will generate the same electrical output for a given incident radiation. Each detector will have a spectral sensitivity characteristic of its photocathode and electron amplification mechanism.

As shown in Figure 1, the two PM tubes were mounted inside the frost chamber: one to monitor the incident radiation (PM 9553) and one to monitor the reflected radiation (PM 6157). There were no optical components between PM 9553 and the frost and likewise for PM 6157.

To measure the frost reflectivity it is only necessary to know the relative sensitivity of the PM tubes since, once the incident radiation (I_0) is measured by PM 9553, this I_0 can be adjusted to what PM 6157 would have measured. A secondary standard (BaSO_4) was employed to determine the hemispherical reflectivity; therefore, it is not required that the PM tubes be calibrated on an absolute base. The relative sensitivity of the PM tubes or cross-calibration must be experimentally determined even though the manufacturer often supplies the quantum efficiency of each PM tube.

The relative sensitivity of the PM tubes was determined by placing the tubes in the frost chamber side by side facing the UV beam. Each tube was moved in and out of the beam and their outputs were divided. This procedure was followed until the wavelength range 1400\AA to 3400\AA was covered.

The cross-calibration was measured before the frosts were grown and then some six months later the cross-calibration was measured again. The second cross-calibration was in poor agreement with the pre-cross-calibration. This discrepancy was of great concern since all of the frost reflectivities had been calculated using the pre-cross-calibration.

It was soon recognized that only one procedure in the calibration scheme had changed from the pre- to post-cross-calibration. The PM 9553 had never been moved from its holder, since it faced the UV beam during the calibration and frost experiments, but the PM 6157 had to be moved to the front flange of the frost chamber in order to record the reflected radiation. During the post-cross-calibration the PM 6157 was repositioned in the holder exactly as it was for the pre-cross-calibration with the one exception of roll orientation.

Upon examining the effect of changing the PM 6157 in roll it was found that a difference in signal output of up to 30 percent resulted. It was suggested that if the UV beam and the PM photocathode was nonuniform the result would be a change in PM tube output with a change in roll position. To establish this fact, the UV beam was stopped down such that a spot approximately $1/16$ " diameter was formed on the face of the PM tube. The PM tube was then moved laterally so

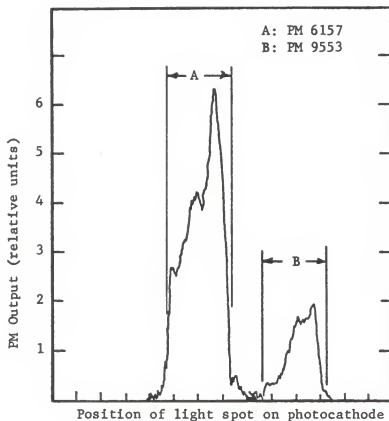


Figure 32. Photomultiplier Photocathode
Nonuniformities

NOTES

Dimensions "A" and "B" correspond to the distance traversed by the 1/16 inch diameter spot of light across the face of each PM tube.

that the 1/16" diameter spot traversed its face. This was done for both PM tubes and the results are shown in Figure 31. The distances labeled "A" and "B" correspond to the distance the spot moved across the face of each PM tube. If the PM photocathodes were uniform this signal would be relatively constant as the spot traversed the face of the tubes. As is clear from the figure this is not the case. The fact that nonuniformities in the photocathodes of the PM tubes were causing the errors in the cross-calibration had thus been established.

To determine the scatter in the cross-calibration values the PM 9553 was left fixed in its holder (the same position as during the frost experiments) while the PM 6157 was changed in roll at 45° intervals. The cross-calibration was measured for all eight positions of the PM 6157. For the various positions there were some overall differences in absolute sensitivity but the important quantity is the difference in relative "spectral" sensitivity. The eight cross-calibration curves were thus normalized at 2000\AA and averaged to establish the final cross-calibration curve. This is shown in Figure 3 with the appropriate error bars.

All of the frost data were reduced again using the post-cross-calibration. Prior to discovering the calibration problem the experimental error was approximately ± 2 percent; however, since no improvement of the UV beam and PM photocathode uniformity could be made the maximum spectral error in the frost photometry was ± 5 percent.

BIBLIOGRAPHY

- Anderson, R. C., J. G. Pipes, A. L. Broadfoot, and L. Wallace, 1969: Spectra of Venus and Jupiter from 1800Å to 3200Å. J. of Atm. Sci., 26, 874-888.
- Anderson, R. C. and J. G. Pipes, 1971: Jovian Ultraviolet Reflectivity Compared to Absorption by Solid Ammonia, J. of Atm. Sci., 28, 1086-7.
- Benford, F., S. Schwarz, and G. P. Lloyd, 1948a: Coefficients of Reflection in the Ultraviolet of Magnesium Carbonate and Oxide, J. of the Optical Society of America, 38, 964-5.
- Benford, F., G. P. Lloyd, and S. Schwarz, 1948b: Coefficients of Reflection of Magnesium Oxide and Magnesium Carbonate, J. of the Optical Society of America, 38, 445-447.
- Billmeyer, F. W., Jr., 1969: Part X: White Reflectance Standards, Optical Spectra, Jan/Feb.
- Black, I. A., L. H. Bolz, F. P. Brooks, F. A. Mauer, and H. S. Peiser, 1958: A Liquid-Helium Cold Cell for Use with an X-ray Diffractometer, J. of Research of the National Bureau of Standards, 61, 367-371.
- Dressler, K. and O. Schnepp, 1960: Absorption Spectra of Solid Methone, Ammonia and Ice in the Vacuum Ultraviolet, J. of Chemical Physics, 33, 270-274.
- Eastman Kodak, 1969: 'Eastman White Reflectance Paint,' Eastman White Reflectance Standard, #JJ-32 (paint) and JJ-31 (standard).
- Fehsenfeld, F. C., K. M. Evenson, and H. P. Broida, 1964: NBS Report #8701, Microwave Discharge Cavities Operating at 2450 MHz.
- Grum, F. and G. W. Luckey, 1968: Optical Sphere Paint and a Working Standard of Reflectance, Applied Optics, 7, 2289-94.
- Harrison, H. and R. I. Schoen, 1967: Evaporation of Ice in Space: Saturn's Rings, Science, 157, 1175-6.

- Kieffer, H. H., 1968: Near Infrared Spectral Reflectances of Simulated Martian Frosts, Dissertation, California Institute of Technology.
- _____, 1969: Reflectance Spectrometer/Environmental Chamber for Frosts, Applied Optics, 8, 2497-2500.
- _____, 1970: Spectral Reflectance of CO₂-H₂O Frosts, J. of Geophysical Research, 75, 501-9.
- Knox, R. S., 1963: Theory of Excitons, Academic Press (Supplement 5).
- Kuiper, G. P., D. P. Cruikshank, and U. Fink, 1970a: The Composition of Saturn's Rings, Sky and Telescope, 39, 14.
- _____, 1970b: (letter to editor), Sky and Telescope, 39, 80.
- Lewis, J. S., 1969: The Clouds of Jupiter and the NH₃-H₂O and NH₃-H₂S System, Icarus, 10, 365-378.
- Mauer, F. A., L. H. Bolz, H. S. Peiser, and H. F. McMurdie, 1972: (private communication, Notes on non-cubic NH₃).
- Owen, T., 1965: Saturn's Ring and the Satellites of Jupiter: Interpretations of Infrared Spectra, Science, 149, 974-5.
- Pilcher, C. G., C. R. Chapman, L. A. Lebofsky, and H. H. Kieffer, 1970: Saturn's Rings: Identification of Water Frost, Science, 167, 1372-3.
- Prinz, G. A., 1972: (private communications), U. S. Naval Research Laboratory.
- Schnepf, O. and K. Dressler, 1960: Absorption Spectra of Solid Xe, Kr, and Ar in the Vacuum Ultraviolet, J. of Chemical Physics, 33, 49-55.
- Seiber, B. A., B. E. Wood, A. M. Smith, P. R. Muller, 1970: Density of Low Temperature Ice, Science, 170, 652-4.
- Smith, A. M., K. E. Tempelmeyer, P. R. Muller, and B. E. Woods, 1969: Angular Distribution of Visible and Near I. R. Radiation Reflected from CO₂ Cryodeposits, AIAA Journal, 7, 2274-80.
- Van De Hulst, H. C., 1957: Light Scattering by Small Particles, John Wiley & Sons, Inc.

- Wallace, L., J. J. Coldwell, and B. D. Savage, 1972: Ultraviolet Photometry from the OAO-III Observations of Venus, Mars, Jupiter, and Saturn Longward of 2000Å, The Astrophysical J., 172.
- Watanabe, K., M. Zelikoff, and E. C. Y. Inn, 1953: AFCRC Tech. Rpt. No. 53-23, Geophys. Res. Paper No. 21.
- Wood, B. E. and A. M. Smith, 1968: Spectral Reflectance of Water and Carbon Dioxide Cryodeposits from .36 to 1.15μ, AIAA J., 7, 1362-1367.
- Wood, B. E., A. M. Smith, J. A. Roux, and B. A. Seiber, 1971: Spectral Infrared Reflectance of H₂O Condensed on LN₂-Cooled Surfaces in Vacuum, AIAA J., 9, 1836-1842.


BIOGRAPHICAL SKETCH

John G. Pipes was born on September 6, 1945, in Gardner, Massachusetts. He graduated from Dan McCarty High School, Ft. Pierce, Florida, in June, 1963. In September, 1963, he entered Indian River Junior College in Ft. Pierce and received the Associate of Arts degree two years later. In September, 1965, he transferred to the University of Florida, where he received the degree of Bachelor of Science in Aerospace Engineering in December, 1967. In January, 1968, he enrolled in the Graduate School of the University of Florida. He spent April and May of 1968 as a visiting graduate student at Kitt Peak National Observatory in Tuscon, Arizona during the preparation of an Aerobee rocket package for the observation of the ultraviolet spectrum of Jupiter.


In June of 1969 he received the Master of Science in aerospace engineering, having done graduate work in planetary atmospheres and engineering optics. From that date until the present he has pursued the degree of Doctor of Philosophy at the University of Florida.

John G. Pipes is married to the former Betty Anne Veber and has two children, Michael, age four, and Pamela, age two.


I certify that I have read this study and that, in my opinion, it conforms to acceptable standards of scholarly presentation and is fully adequate, in scope and quality, as a dissertation for the degree of Doctor of Philosophy.


Roland C. Anderson, Chairman
Associate Professor of Aerospace
Engineering

I certify that I have read this study and that, in my opinion, it conforms to acceptable standards of scholarly presentation and is fully adequate, in scope and quality, as a dissertation for the degree of Doctor of Philosophy.


Alex G. Smith
Professor of Physics and Astronomy


I certify that I have read this study and that, in my opinion, it conforms to acceptable standards of scholarly presentation and is fully adequate, in scope and quality, as a dissertation for the degree of Doctor of Philosophy.


Alex E. S. Green
Graduate Research Professor in
Physics and Astronomy

I certify that I have read this study and that, in my opinion, it conforms to acceptable standards of scholarly presentation and is fully adequate, in scope and quality, as a dissertation for the degree of Doctor of Philosophy.


Bernard M. Leadon
Professor of Aerospace Engineering

I certify that I have read this study and that, in my opinion, it conforms to acceptable standards of scholarly presentation and is fully adequate, in scope and quality, as a dissertation for the degree of Doctor of Philosophy.


David T. Williams
Professor of Aerospace Engineering

I certify that I have read this study and that, in my opinion, it conforms to acceptable standards of scholarly presentation and is fully adequate, in scope and quality, as a dissertation for the degree of Doctor of Philosophy.



Mark H. Clarkson
Professor of Aerospace Engineering

This dissertation was submitted to the Dean of the College of Engineering and to the Graduate Council, and was accepted as partial fulfillment of the requirements for the degree of Doctor of Philosophy.

June, 1972



Dean, College of Engineering

Dean, Graduate School

